

This article was downloaded by:

On: 21 January 2011

Access details: *Access Details: Free Access*

Publisher *Taylor & Francis*

Informa Ltd Registered in England and Wales Registered Number: 1072954 Registered office: Mortimer House, 37-41 Mortimer Street, London W1T 3JH, UK



International Reviews in Physical Chemistry

Publication details, including instructions for authors and subscription information:

<http://www.informaworld.com/smpp/title~content=t713724383>

Bent bonds probed by ligand-field analysis

M. J. Duer^a; N. D. Fenton^a; M. Gerloch^a

^a University Chemical Laboratories, Cambridge, England

To cite this Article Duer, M. J. , Fenton, N. D. and Gerloch, M.(1990) 'Bent bonds probed by ligand-field analysis', *International Reviews in Physical Chemistry*, 9: 3, 227 – 280

To link to this Article: DOI: 10.1080/01442359009353247

URL: <http://dx.doi.org/10.1080/01442359009353247>

PLEASE SCROLL DOWN FOR ARTICLE

Full terms and conditions of use: <http://www.informaworld.com/terms-and-conditions-of-access.pdf>

This article may be used for research, teaching and private study purposes. Any substantial or systematic reproduction, re-distribution, re-selling, loan or sub-licensing, systematic supply or distribution in any form to anyone is expressly forbidden.

The publisher does not give any warranty express or implied or make any representation that the contents will be complete or accurate or up to date. The accuracy of any instructions, formulae and drug doses should be independently verified with primary sources. The publisher shall not be liable for any loss, actions, claims, proceedings, demand or costs or damages whatsoever or howsoever caused arising directly or indirectly in connection with or arising out of the use of this material.

Bent bonds probed by ligand-field analysis

by M. J. DUER, N. D. FENTON and M. GERLOCH

University Chemical Laboratories, Lensfield Road,
Cambridge CB2 1EW, England

Bonding electron density need not be distributed symmetrically about the line-of-centres of bound atoms. This review describes how recent ligand-field analysis has been able to detect such circumstances and other forms of misdirected valency. Eight groups of analyses, comprising detailed studies of 25 individual complexes, involve quantitative reproductions of paramagnetic susceptibilities, electron spin resonance g^2 tensors, and 'd-d' transition energies, absorbances and rotatory strengths. These careful studies provide a showcase for the reach and power of contemporary ligand-field models as well as a level of detailed insight into transition-metal bonding that is not readily available by other means. The examples given here are prefaced with brief reviews of the parametric structures of the ligand-field method. These refer to the cellular ligand-field models for both energies and intensities of electronic transitions. An indication of how calculations of magnetic properties, transition energies, spectral intensities and circular dichroism—all within a d^n basis—are implemented in practice is included.

1. Why might bonds be bent?

A widespread, if not universal, concept in chemical bonding is the notion of directed valency. A valence bond description, for example, of methane begins with a tetrahedral arrangement of four hydrogen atoms around the central carbon atom as that of closest packing, followed by the construction of carbon sp^3 hybrids directed along the lines of atomic centres and making optimal overlap with the hydrogen 1s orbitals. Moving then to the ideas of Gillespie and Nyholm (1957), now called VSEPR theory, attention focuses upon interelectron repulsion energies between the occupied bond orbitals; fatter bonds repel more than thinner ones, and so on. Regardless of whether these ideas are expressed in the language of valence bond theory or of molecular orbital theory, one recognizes that energies associated with both overlap and interelectron repulsion must be considered.

While overlap terms are most important near the middle of bonds—in regions most occupied by orbitals from each bound atom—electron–electron repulsion energies will tend to be greatest near atomic centres where the electrons are closest together. Considering the single bonds in a methane derivative, for example, these repulsion energies will favour a tetrahedral disposition of the bond electron pairs. In that the electronegativities of the four surrounding atoms may differ amongst themselves, differential electron donation or withdrawal may render inexact the tetrahedral electron arrangement close to the central atom. If the outer atoms are free to move, they will do so in order to maximize overlap and so establish bonds that concentrate along each atom–atom vector. So while the geometry may not be exactly tetrahedral, the bonds will be 'straight'. But the non-central atoms may not be free to move in this way. They may be the donor atoms of a chelate, for example, or be part of some ligand group that is restrained elsewhere by reason of steric forces, hydrogen bonding, crystal packing, and so on. In these circumstances, while the best possible overlap may be quite

sufficient to maintain the bond, it need not be concentrated exactly along the line of atomic centres. There will result a bent bond.

The question now arises as to how bent bonds might be detected experimentally. Diffraction methods come first to mind, often being called 'direct', but they involve modelling just like any other. Mapping valence electron density by X-ray deformation density analysis or valence spin density by polarized neutron diffraction, for example, is very difficult; especially so in regions close to the metal in transition-metal complexes. Nevertheless, a number of such studies do seem to have identified bent bonds. The coordination about the metal in $\text{CuSO}_4 \cdot 5\text{H}_2\text{O}$ crystals, for example, includes interactions with water ligands in two different ways (Varghese and Maslen 1985). Two of the water ligands appear well described as sp^2 hybridized in that the Cu–O vector bisects the H–O–H angle. The deformation Fourier difference map reveals electron density lying virtually exactly along the Cu–O vectors for these ligations. By contrast, the remaining copper–water ligations show little symmetry; the hydrogen atoms are involved in unequal hydrogen bonding and the Cu–O vector neither bisects the \angle H–O–H angle nor lies in the HOH plane. The deformation density map here shows regions of electron density that lie to one side of the corresponding Cu–O vectors roughly towards positions that one might expect to be occupied by an oxygen sp^3 hybrid orbital. Similarly, the spin density in the CoCl_4^{2-} ion in Cs_3CoCl_5 as determined by polarized neutron diffraction analysis (Chandler *et al.* 1982), is concentrated rather more in an exact T_d arrangement than are the cobalt–chlorine vectors themselves.

The present article focuses upon the contribution that modern ligand-field analysis can bring to the characterization of bent bonding in transition-metal complexes. Studies of the spectral and magnetic properties of a score or more d block compounds have demonstrated the effects of bent bonds and other electron distributions describing misdirected valency. While supporting and elaborating the discussions above, they simultaneously illuminate the increasing reach of contemporary ligand-field analysis from magnetic anisotropy to spectral intensities and circular dichroism.

2. Ligand-field theory

2.1. The scope of ligand-field analysis

Ligand-field analysis today is more wide-ranging, more subtle and more successful than ever. Because it is parametric and because it began so many decades ago, many see it as the weak sister of computational molecular-orbital theory. Certainly it does not have the scope of *ab initio*, or even approximate, molecular-orbital models but it is tailored, by Nature, ideally to its particular tasks. One can now model and *quantitatively* reproduce the magnitudes and orientations of paramagnetic susceptibilities and of electron spin resonance (ESR) g values; 'd–d' (or 'f–f') transition energies, absorption intensities and the rotatory strengths recorded in the circular dichroism (CD) experiment: all this for single-centre transition-metal complexes of any coordination geometry, any coordination number, or any dⁿ (or fⁿ) formal configuration. This success story is essentially unbroken to date except in so far as high molecular symmetry or limited data might render successful analyses ambiguous to a greater or lesser extent. As chemists, we contend that the mere reproduction of all these experimental data, however difficult that might be on occasion, is of little interest unless the model parameters that establish it also provide a commentary upon chemical structure and bonding that is readily comprehensible and pictorial, and which *consistently* correlates with chemical common sense as established by other means. By

and large, this has been, and continues to be, achieved, albeit at a semi-quantitative level. There is no contradiction between the quantitative reproduction of experiment and the more qualitative interpretations offered by the analysis, for the structure of the ligand-field method is such as to separate those quantities which are calculable—within the central assumptions of the approach—from those which, in common with computational molecular-orbital models, are not. The best ligand-field models are those which best achieve that separation. Of these, those exploiting a principle of spatial superposition offer the greatest chemical transparency.

The cellular ligand-field (CLF) model implements these aims. While inspired by the angular overlap model (AOM), and sharing with it parameter nomenclature, the CLF approach rests upon quite different principles and offers different parameter interpretations and hence chemical conclusions: often the differences are small, but in a significant number of analyses they are not. The background for these assertions is reviewed briefly in the next sections. In its most basic form, the CLF expresses the ligand field in a complex as a sum of local fields with each usually, though not invariably, associated with a single metal–ligand interaction. These local ligations are usually viewed within an appropriate *pseudo-symmetry*: $C_{\infty v}$ for a metal–halogen interaction, for example, or C_{2v} if ‘ π ’ bonding is to be differentiated between the planes perpendicular to the metal–donor vector. While it has always been recognized—in the CLF approach as in its AOM precursor—that the adoption of the pseudo-symmetry approximation is made in the interests of tractability, these simplifications have been repeatedly justified by the ability of the scheme to reproduce experiment and to do so with parameter values that accord with general chemical and bonding ideas. Occasionally, however, this simple representation of a local, or cellular, ligand field has proved inadequate in both these respects. The failures are always associated with lower, local pseudo-symmetry; in particular, when electron density for the ligation is aptly described by C_s symmetry. In these circumstances, the local ligand-field arises in part from electron density that is unsymmetrically situated with respect to the metal–donor axis. In short, these failures of the ligand-field model have resulted from explicit neglect of misdirected valency. Bent bonds are one form of misdirected valency.

The present article describes how refinement of the CLF approach has removed these problems so that ‘less ideal’ coordinations are now treated on the same footing as those more simple ligations; and, in so doing, has provided a clearer insight into the nature of directed bonding.

2.2. A bonding probe

Crystal-field theory (CFT) addressed the perturbation of transition-metal *d* (or *f*, for lanthanides) electrons in a classical potential provided by point-charges or electric dipoles, for example, surrounding a metal atom. The focus was the splitting of the terms of a free-ion d^n configuration and its considerable successes derived from the exploitation of symmetry and group theory. *Quantitative* calculations of the magnitudes of term splittings, like $10Dq$, within a variety of models yielded widely differing results. All in all, they failed miserably to reproduce experiment. Ligand-field theory (LFT) retains the angular parts of CFT but subsumes the radial parts within an effective operator technique. Ligand-field splittings are deemed to account implicitly for the covalency that undoubtedly exists in the object systems of study. Nevertheless, ligand-field theory still focuses upon the splittings of d^n (or f^n) basis functions. It thus seeks to provide an account of spectroscopic and magnetic properties in transition-metal complexes by explicit reference only to the *d* (*f*) electrons. LFT developed as it did

surely because of its empirical or phenomenological success, repeated countless times then and since, based upon the view of a d^n configuration subject to an *effective* ligand-field potential. So far as ligand-field properties in complexes are concerned, we look at the d^n configuration of the metal rather than at some other configuration composed of s, p and d functions. Viewed as procedures, the CFT and LFT methods entail the diagonalization of pure d^n ($l=2$) or pure f^n ($l=3$) many-electron states under explicit or implicit Hamiltonians, as follows:

$$\mathcal{H}_{\text{CF}} = \sum_{i < j} \frac{e^2}{r_{ij}} + \sum_i V_{\text{CF}}(\mathbf{r}_i) + \zeta_0 \sum_i \mathbf{l}_i \cdot \mathbf{s}_i, \quad (1)$$

$$\mathcal{H}_{\text{LF}} = \sum_{i < j} U(i, j) + \sum_i V_{\text{LF}}(\mathbf{r}_i) + \zeta \sum_i \mathbf{l}_i \cdot \mathbf{s}_i. \quad (2)$$

The two-electron ‘interelectron repulsion’ energies are evaluated within the usual Slater–Condon–Shortley theory, being parameterized by *free-ion*, F_k (or equivalent Racah) parameters in the crystal-field model or by freely variable F_k parameters for the given complex in the ligand-field approach. The difference derives from the presumption of known fixed *radial* forms for the d functions in CFT but of unknown forms in LFT. That same distinction accounts for the use of the free-ion, spin–orbit coupling coefficient, ζ_0 , in CFT but of the variable parameter, ζ , in LFT. Finally, V_{CF} takes the form of an explicit function of geometry and charge distribution while V_{LF} is defined merely as a one-electron operator.

That V_{LF} is thus deemed to subsume covalency has all too frequently directed attention almost exclusively upon overlap between metal d orbitals and those of the ligand. That is understandable, perhaps, given the development of bonding ideas in inorganic chemistry at large but it proves to be poor emphasis. The fact remains that the efficacy of the ligand-field method, together with the primacy of the d^n configuration, separates the d (f) electrons from the rest. The separation need not, and undoubtedly is not, total but it identifies a starting point. The situation is reminiscent of π electron theory in organic chemistry in which attention is focused upon the π electrons within the environment of all others. In effect, Nature has provided these approximate factorizations in both areas of the periodic table. Had it not, neither π electron theory nor ligand-field theory would have successfully reproduced experiment and survived so long in chemical modelling. During the past few years, Gerloch *et al.* (1981), Woolley (1981, 1985, 1987), Gerloch (1983, 1987) and Gerloch and Woolley (1984) have examined the underlying structure of ligand-field theory in terms of quantum chemistry at large. These studies view LFT as a projection of the complete many-electron molecular Hamiltonian on to a d orbital basis that establishes the \mathcal{H}_{LF} of (2) as an effective Hamiltonian which is reasonably constant throughout the ‘ligand-field regime’ of low-lying d states. The formalism of this viewpoint has been developed sufficiently to provide the basis for a computational study, although that has not been carried out; firstly, because it would be every bit as difficult as the more usual *ab initio* calculations in such molecules and these are known to be inadequate at the level of accuracy required in ligand-field studies, and secondly because the point of these theoretical studies was to discover what circumstances permit the success of the ligand-field approach. In essence, these circumstances are that the d electrons in transition-metal complexes, like the f electrons in lanthanides, are largely uncoupled from the rest; and this can only come about if overlap between d orbitals and the rest is small.

We propose that a useful working view of electronic interactions in transition-metal complexes to be as follows (Gerloch 1990). In higher oxidation state complexes of the Werner type, but not in low oxidation state ones like carbonyls, the d electrons are little involved in the valence shell. Bonding with ligands takes place between ligand functions and metal s and/or p orbitals, a process that includes charge redistribution between all ligands and the metal in response to the electroneutrality principle. The radial form of the metal d function changes during this process. As a secondary perturbation, the d electrons interact with all else but mostly with the bonding electrons, to which they are closest. Their energies become differentiated, they mix up amongst themselves, but their ultimate mixing with the bond orbitals is slight. In the angular overlap model, a single molecular orbital scheme predicts that d orbital energy shifts are proportional to the squares of overlap integrals between estimable metal d orbitals and appropriate ligand functions, but this prediction often fails. In the cellular ligand-field approach, one can conclude that those energy shifts are roughly proportional to the squares of overlaps between mean d orbitals and local bond orbitals, built, as described above, from all valence shell functions. But we are to recognize that the forms of neither mean d orbitals (those resulting from the mean central field in the formed complex) nor the bond orbitals are readily guessable. In this way, ligand-field theory is excused the tasks of bonding theory. The energies and characters of the ligand-field d orbitals are parameterized within the ligand-field method, using (2) and other operators to be discussed, however, and so act as probes of the underlying bonding. Intelligent guessing from the accumulation of actual analytical results about correlations between ligand-field parameter values and chemical bonding is entirely possible. Being undertaken separately and subsequently, its quantitative limitations do not invalidate the analytical processes themselves.

2.3. The cellular superposition

Ligand-field calculations involve the diagonalization of the ligand-field Hamiltonian, \mathcal{H}_{LF} of (2), within a basis of functions spanning the whole or part of the appropriate d^n configuration. Only the ligand-field potential V_{LF} , carries information about the molecular geometry and the spatial decomposition to which the CLF refers concerns just that part of \mathcal{H}_{LF} . Taking the molecule as a whole, we consider the matrix \mathbf{V} of the operator V (dropping the LF subscript, for simplicity) within the set of d orbitals $\{d\}$ defined with respect to an arbitrary, but fixed, global frame:

$$(\mathbf{V})_{ij} = \langle d_i | \hat{V} | d_j \rangle; \quad i, j = 1, \dots, 5. \quad (3)$$

Let us divide up the physical space around the metal atom into N discrete and contiguous regions. The potentials, \hat{v}^c , in each region or cell (c), sum to reform the total potential \hat{V} :

$$\hat{V} = \sum_{c=1}^N \hat{v}^c. \quad (4)$$

Similarly, matrix elements of the cellular potentials are related to those of the global potential by

$$(\mathbf{V})_{ij} = \sum_{c=1}^N \langle d_i | \hat{v}^c | d_j \rangle = \sum_{c=1}^N (\mathbf{v}^c)_{ij}. \quad (5)$$

Each Hermitian cellular matrix v^c can be brought to diagonal form by a unitary transformation,

$$\mathbf{R}^c v^c \mathbf{R}^{c\dagger} = \mathbf{e}^c. \quad (6)$$

where \mathbf{e}^c is a 5×5 diagonal matrix with diagonal matrix elements $\{e_k^c\}$ and the unitary matrices \mathbf{R}^c ,

$$\mathbf{R}^c \mathbf{R}^{c\dagger} = \mathbf{R}^{c\dagger} \mathbf{R}^c = \mathbf{1}. \quad (7)$$

are associated with each individual cell, c . The same result can be achieved for each cell by constructing cellular orbitals, $\{d^c\}$,

$$\langle d_k^c | = \sum_i^5 (\mathbf{R}^c)_{ki} \langle d_i |, \quad (8)$$

that diagonalize the cellular potentials \hat{v}^c directly, so that the $\{e_k^c\}$ of (6) are given as matrix elements of the local potential within the local basis

$$e_k^c = \langle d_k^c | \hat{v}^c | d_k^c \rangle. \quad (9)$$

Substitution of (6), (8) and (9) into (5) yields the 'master equation' of the cellular ligand-field model:

$$(\mathbf{V})_{ij} = \langle d_i | \hat{V} | d_j \rangle = \sum_c^N \sum_k^5 (\mathbf{R}^c)_{ik}^r (\mathbf{R}^c)_{kj} e_k^c. \quad (10)$$

At this point it is important to emphasize that these simple formal manipulations involve no physical assumptions, once given the starting point that it is useful to consider an object like the effective ligand-field potential. The cellular equation (10) only acquires physical—and hence chemical—utility as we endow two aspects of the foregoing transformation with general representational significance.

The first of these concerns the spatial decomposition of the potential in (4). While it is trivial to express the global potential as a sum of local parts, it is a matter of assertion to suppose that the sources of each local potential are situated locally. That would not be the case for a simple collection of point negative charges around a metal atom, for example, for the potential in any one cell would clearly comprise contributions from all those charges whether they were located in that cell or not. We have argued elsewhere (Gerloch and Woolley 1984), however, that for more realistic charge distributions, dielectric screening can be expected vastly to decrease contributions from adjacent or more distant cells. However reasonable the assumption, it is nevertheless important to recognize that the CLF approach is partly built on the idea that local potentials are dominated by local charge densities. In particular, and recalling the discussion in the preceding section, it is supposed that each local potential arises from the local bonding electrons. That being so, we are lead naturally to the second major assumption of the CLF approach.

This concerns the selection and significance of the unitary matrices, $\{\mathbf{R}^c\}$ in (6), and the number of cells used in the spatial decomposition. These choices are to be made whilst satisfying two criteria; that \mathbf{R}^c ultimately diagonalizes v^c , as in (6), and that the local electron density in a cell dominates the potential in that cell. These conditions are most obviously satisfied if there is one cell per ligation, roughly centred about the metal-donor axis; and when the \mathbf{R}^c are identified with rotation matrices expressing the relationship with the global frame of local axes chosen to correspond with elements of the pseudo-symmetry of the local electron density. These most usual circumstances are

well illustrated by a metal–pyridine ligation of local pseudo-symmetry C_{2v} with axes chosen parallel to the metal–nitrogen axis (z) and parallel (x) and perpendicular (y) to the pyridine plane as shown in figure 1. The local bonding is presumed to be aptly differentiated and labelled by σ , π_x and π_y , in this frame, as is the ensuing local ligand-field potential probed by the locally referred d orbitals: in turn, similar labels are taken by the local $\{e_k^c\}$ of (9) which parameterize the local, diagonal ligand-field matrix. In an obvious nomenclature, the non-zero elements of the local v^c matrix are given by

$$\left. \begin{aligned} e_{\sigma}^c &= \langle d_{z^2}^c | v^c | d_{z^2}^c \rangle, & e_{\pi_x}^c &= \langle d_{xz}^c | v^c | d_{xz}^c \rangle, \\ e_{\pi_y}^c &= \langle d_{yz}^c | v^c | d_{yz}^c \rangle, & e_{\delta_{xy}}^c &= \langle d_{xy}^c | v^c | d_{xy}^c \rangle, \\ e_{\delta_{x^2-y^2}}^c &= \langle d_{x^2-y^2}^c | v^c | d_{x^2-y^2}^c \rangle, \end{aligned} \right\} \quad (11)$$

although, because of assumed negligible M–L δ bonding and other reasons elaborated elsewhere, the last two are invariably set to zero. For a metal–halogen ligation with local pseudo-symmetry $C_{\infty v}$, $e_{\pi_x}^c$ is set equal to $e_{\pi_y}^c$ and the directions chosen for x and y are unimportant.

There are two sets of circumstances in which the choices made above are inadequate. One, to which we return shortly, is the subject of the present article. The other concerns the number of cells, and hence sets of $\{e^c\}$ parameters, into which the global potential is divided. In coordinationally sparse complexes it has proved necessary, by empiricism in the first instance, to assign cells to coordinationally void regions of space. Ultimately this is because a coordinationally void cell need not be empty of all sources of potential. In effect, complementary parts of the set of bond orbitals elsewhere spill over into these ligand-free regions. The neglect of coordination voids in these circumstances means that sources for a given cellular potential arise from more than one region of space—the ‘real bond’ and adjacently, the ‘overspill’. A choice of \mathbf{R}^c based upon the environment of the ‘real bond’ will not diagonalize the potential arising from these two sources together. In practical terms, coordinationally void cells are assigned to the regions above and below the coordination plane in planar species, for example, and parameterized by negative e_{σ}^c values. When that is done, parameter values for the real ligations in such complexes fit well with general experience in ligand-field analysis. Theoretical reasons for the negative strength of the ligand field of a coordination void—a concept quite foreign to the molecular-orbital-based AOM—have been given (Gerloch 1983, Gerloch and Woolley 1984) and the behaviour explored empirically (Deeth and Gerloch 1984) throughout a wide range of complexes. Only because our focus in this article lies elsewhere do we not describe this more fully here.

The other circumstance in which the parameterization scheme above is inadequate is the central issue of this review. The identification of the unitary transformation matrices \mathbf{R}^c with rotation matrices referring to frames defined by the local bonding *pseudo*-symmetry is predicted on an assumption that the local bonding electron

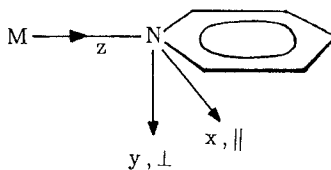
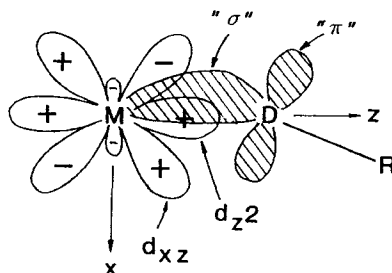


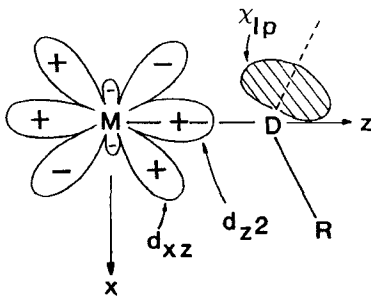
Figure 1. Local C_{2v} pseudo-symmetry for a metal–pyridine ligation.

density distribution can be guessed sufficiently well to define local axes relative to which the local potential will be diagonal. Ligations of two kinds deny that precondition. They are illustrated in figure 2 and belong to the lower pseudo-symmetry C_s . While even lower local symmetry can occur in practice, the issues addressed here are adequately covered within this group. Figure 2(a) illustrates the case of local bent bonding such that the ' σ ' bond lies more to one side of the metal-donor atom vector than the other. Similar misdirection of the ' π ' bond may well occur and is included automatically in the discussion below. At this stage we might suppose that the origin of such bent bonding lies in forces concentrated further out on the ligand, in the group R, perhaps due to chelate ring strain or crystal packing forces. We discuss the origins of bent bonding more fully in later sections. For the moment, we recognize that the appropriate choice of local x and z axes for the usual cellular construction cannot be made *a priori*. Certainly one particular orientation of the local frame will correspond to a locally diagonal ligand-field matrix but we cannot guess which. If we choose the frame shown in the figure, in which z is directed from the metal to the donor atom, we must simultaneously relinquish the usual demand of the CLF that \mathbf{R}^c will diagonalize the local matrix. And that is just what we do. We trade certainty, by choosing local axes as in figure 2, for a non-diagonal ligand-field matrix, and hence an extra parameter:

C_{2v} pseudo-symmetry	C_s pseudo-symmetry	
d_{z^2} d_{xz} d_{yz}	d_{z^2} d_{xz} d_{yz}	
d_{z^2} e_σ 0 0 d_{xz} 0 $e_{\pi x}$ 0 d_{yz} 0 0 $e_{\pi y}$	d_{z^2} e_σ $e_{\pi\sigma}$ 0 d_{xz} $e_{\pi\sigma}$ $e_{\pi x}$ 0 d_{yz} 0 0 $e_{\pi y}$	(12)



(a)



(b)

Figure 2. Misdirected valence (a) from bent bonding, and (b) from a 'non-bonding' lone pair.

The Greek labels used in the right-hand matrix do not, of course, label irreducible representations of the C_s group. The new off-diagonal parameter $e_{\pi\sigma}$ accounts for the fact that *both* d_{z^2} and d_{xz} orbitals in figure 2 can interact with the (shaded) bent bond. From the point of view of the CLF matrix, and hence, for the whole process of ligand-field analysis, other sources of off-axis electron density give rise to entirely analogous consequences. In particular, the presence of a formally non-bonded lone pair on the donor atom, as in figure 2(b), constitutes another form of what may be called 'misdirected valency'. In the analyses described later, both physical sources for the off-diagonal $e_{\pi\sigma}$ parameter frequently occur together.

2.4. The sign of the $e_{\pi\sigma}$ parameter

It has been shown elsewhere that the CLF matrix elements are dominated by a so-called 'dynamic' contribution of the form

$$(\mathbf{v}^c)_{ij} = \langle d_i^c | \hat{v}^c | d_j^c \rangle \sim \sum_x \left\langle d_i^c \left| \frac{\mathcal{H}^{(1)} | \chi \rangle \langle \chi | \mathcal{H}^{(1)} |}{\epsilon_d - \bar{\epsilon}_x} \right| d_j^c \right\rangle. \quad (13)$$

This expression is derived, as sketched in section 2.2., from consideration of the dynamics of d electrons in the field of all other particles in the complex. Full and careful presentations have been given elsewhere: here we give the briefest of summaries.

Density functional theory establishes that the electron density, ρ , in the ground state of a molecule can be expressed completely as a simple sum over populated 'best' orbitals. Sadly, of course, no simple recipe exists to establish the precise forms of these best orbitals. Let us, however, notionally subtract from the true density, ρ , a d electron density, ρ_d , to be defined self-consistently below. We write a one-electron Hamiltonian, \mathcal{H} , whose potential energy term, V , is a functional of $(\rho - \rho_d)$ and refers to its eigenfunctions $\{\psi\}$ given by

$$(\mathcal{H} - E_n)\psi_n = 0; \quad \mathcal{H} = T + V, \quad (14)$$

as ligand-field orbitals. Now V , being a function of electron density throughout the molecule, is non-spherical. Taking $\langle V \rangle$ as the spherical, or mean, part of V , we can divide up the ligand-field orbitals as eigenfunctions of corresponding spherical and aspherical parts of \mathcal{H} :

$$\mathcal{H} = \mathcal{H}^{(0)} + \mathcal{H}^{(1)} \quad (15)$$

$$\mathcal{H}^{(1)} = V - \langle V \rangle \quad (16)$$

$$\mathcal{H}^{(0)} = T + \langle V \rangle. \quad (17)$$

We define a basis of orbitals as solutions to the central-field Hamiltonian, $\mathcal{H}^{(0)}$:

$$\mathcal{H}^{(0)}\phi_i = (T + \langle V \rangle)\phi_i = \epsilon_i\phi_i, \quad (18)$$

with

$$\phi_i(\mathbf{r}) = R_{nl}(r)Y_m^l(\theta, \phi), \quad (19)$$

and take those with $l=2$ as the d orbitals to be used in ligand-field calculations. The electron density associated with the occupation of these d orbitals is the ρ_d subtracted in the step above. The purpose of this cyclic manoeuvre is to prevent the ligand-field d orbitals interacting with each other as part of the effective ligand-field potential, for that is always dealt with separately in ligand-field theory within the 'interelectron repulsion' operator $U(i,j)$ of (2).

With this brief review of what, in part, lies behind the expression (13) for the CLF parameters, we can now identify the quantities in (13). The $\{d^e\}$ are the locally referred $l=2$ functions of (19); we call them the 'mean d orbitals' of the complex and we note that their radial form, $R_{n,2}(r)$, varies from complex to complex. Their energy under $\mathcal{H}^{(0)}$ is ϵ_d . $\mathcal{H}^{(1)}$ is the aspherical part of the potential in the complex, given by (16). The χ are locally-referred functions built from all orbitals except the d orbitals of (19), with energies, $\bar{\epsilon}_\chi$, given by the expectation values, $\langle \chi | \mathcal{H} | \chi \rangle$. Contributions to the integrals (13) will be dominated by those χ which are spatially proximate to the electron density dominating $\mathcal{H}^{(1)}$ and with energies closest to ϵ_d . In short, the CLF parameters are expected to be dominated by the χ describing the local *bond orbitals* in the complex. This is the origin of our assertion that ligand-field matrix elements probe the bonds in complexes.

In the case of diagonal CLF e parameters, (13) takes the form, ($\lambda = \sigma, \pi_x, \pi_y$),

$$e_\lambda \sim \sum_\chi \left\langle d_\lambda \left| \frac{\mathcal{H}^{(1)}|\chi\rangle\langle\chi|\mathcal{H}^{(1)}}{\epsilon_d - \bar{\epsilon}_\chi} \right| d_\lambda \right\rangle, \quad (20)$$

$$= \sum_\chi \frac{|\langle d_\lambda | \mathcal{H}^{(1)} | \chi \rangle|^2}{\epsilon_d - \bar{\epsilon}_\chi}. \quad (21)$$

The numerator in (21) is necessarily real and positive and so the signs of all diagonal CLF parameters are determined by the signs of the denominators ($\epsilon_d - \bar{\epsilon}_\chi$). If the bond orbital lies below the mean d orbital, the contribution to e_λ is positive and we refer to a ligand λ -donor. The definition of donor/acceptor function here thus refers to the relative energies of bond orbitals and mean d orbitals *after* formation of the complex. Most often, only one local bond orbital will be sufficiently close in energy to the d orbitals to make a significant contribution to the sum in (21). Sometimes there may be two: for example, for π ligations involving energetically close HOMO- and LUMO-like functions (π and π^*). All in all, however, the signs of diagonal CLF parameters are determined by the donor or acceptor nature of the ligand.

The situation is different for the off-diagonal $e_{\pi\sigma}$ parameter, given by

$$e_{\pi\sigma} \sim \sum_\chi \left\langle d_{xz} \left| \frac{\mathcal{H}^{(1)}|\chi\rangle\langle\chi|\mathcal{H}^{(1)}}{\epsilon_d - \bar{\epsilon}_\chi} \right| d_{z^2} \right\rangle. \quad (22)$$

Here the sum is over just one term when χ is the lone pair of figure 2 (b) and ($\epsilon_d - \bar{\epsilon}_\chi$) will be positive: for the bent bonding in figure 2 (a), the sum is over the ' σ ' and ' π ' bent bonds. In either case, the sign of $e_{\pi\sigma}$ will be determined additionally by the numerator, for the functions in bra and ket of (22) may, or may not, be in phase. The sign of the numerator depends upon the direction of bent bonding; that is, the quadrant towards which the bent bond is displaced, as now discussed.

Misdirected valency is represented in the local frame by the matrix element $e_{\pi\sigma} = \langle d_{z^2} | v_{LF}^e | d_{xz} \rangle$, where, from (22),

$$v_{LF}^e = (\mathcal{H}^{(1)}|\chi\rangle\langle\chi|\mathcal{H}^{(1)})/(\epsilon_d - \bar{\epsilon}_\chi). \quad (23)$$

Using the conventions of Brink and Satchler (1968), which are followed in all analyses described in this article, $e_{\pi\sigma}$ is related to a multipole expansion of the local ligand-field matrix elements by equation (9.37) of Gerloch (1983):

$$e_{\pi\sigma} = -\left(\frac{5}{2\pi}\right)^{1/2} c_{21} - \left(\frac{5}{12\pi}\right)^{1/2} c_{41}. \quad (24)$$

Consider the case of misdirected valency associated with the lateral displacement of a bond or lone pair into the negative quadrant of the local frame as in figure 2. Let an incremental part of the local potential, v_{LF}^c , sensed by the metal d orbitals, and deriving from that misplaced electron density and Hamiltonian $\mathcal{H}^{(1)}$, be represented as in figure 3. Relative to the frame $x'z'$, that increment, Δv_{LF}^c , will take the form, when expanded as a series of spherical harmonics,

$$\Delta v_{LF}^c(x'z') = c_{20} Y_0^{(2)} + c_{40} Y_0^{(4)}, \quad (25)$$

with c_{20} and c_{40} both real and positive. That same incremental potential, expressed relative to the fixed, local frame xz is given by

$$\Delta v_{LF}^c(xz) = c_{21} Y_1^{(2)} + c_{41} Y_1^{(4)} + \text{others}, \quad (26)$$

where

$$c_{21} = d_{10}^{(2)}(\theta) c_{20}, \quad (27)$$

$$c_{41} = d_{11}^{(4)}(\theta) c_{40}. \quad (28)$$

Here θ is the (positive) angle of rotation required to transform $x'z'$ into xz , and the rotation matrix elements, $d_{m'm}^{(j)}(\beta)$, are defined for the rotation of a function as by Brink and Satchler. For a small rotation such that $\theta < \pi/2$, $d_{10}^{(2)}(\theta)$ and $d_{10}^{(4)}(\theta)$ are both negative numbers. The same result applies for all small θ values and hence for all increments of the potential v_{LF}^c . So while the appropriate weighted mean θ value for a real misdirected valence is beyond guessing, by comparison with (24), we know that for misdirected valency in the negative xz quadrant, as shown, positive values are to be assigned† to the $e_{\pi\sigma}$ parameter. Conversely, bent bonds or lone pairs lying close to the positive local x axis are to be assigned negative $e_{\pi\sigma}$ values. These signs should all be reversed for misdirected valency associated with ligand acceptors: no real examples of these have been studied to date.

Finally, note that the extra terms mentioned in (26) would be equivalenced by off-diagonal matrix elements like $\langle d_{z^2} | v_{LF}^c | d_{xy} \rangle$ or $\langle d_{z^2} | v_{LF}^c | d_{x^2-y^2} \rangle$. These are explicitly neglected in our account of misdirected valency, essentially because of the minimal overlap that is to be expected with d_δ orbitals when the magnitude of θ and any misdirected valency is small.

2.5. Analytical procedures

While this is not the place to describe the full process of ligand-field analysis, it does seem appropriate to indicate how the wide variety of experimental data to be reviewed are exploited to form views of electron density distribution.

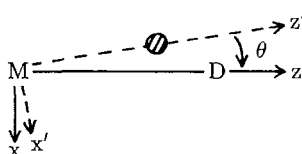


Figure 3. The shaded area represents an incremental source of the local potential.

† The same conclusion was arrived at by incorrect means by Deeth *et al.* (1987a). All analyses reported by us remain valid, however.

All calculations involve the diagonalization of a d orbital basis, expressed as some or all of the free-ion terms arising from an appropriate d^n configuration, under the ligand-field Hamiltonian (2) discussed in section 2.2. The block diagram in figure 4 summarizes the main parts of our CAMMAG3 (1989) suite of programmes which are encoded to implement general ligand-field analysis (see also Gerloch (1983), chap. 10). Using fixed data for the chosen basis and structural parameters to define reference frames for each ligation or coordination void, matrices for each of the operators in (2) as well as for spin- and orbital-angular momentum are computed in the form $\langle LSJM_J | \text{Op} | L'S'J'M_J \rangle$. This much constitutes the SETUP part of the computation and is executed only once. Then, in the RUN programme, a copy of each matrix for (2) is multiplied by a starting energy parameter: F_2, F_4 —or the equivalent B, C —for interelectron repulsion; ζ for spin-orbit coupling; and $\{c_{kq}\}$ for the global ligand-field potential expressed as a multipole expansion and computed from local CLF $\{e\}$ parameters using standard expressions. These matrices are summed and diagonalized numerically to yield eigenvalues, and eigenvectors expressed as combinations of the original d orbital basis. From these are computed the various properties of interest via the programme routes labelled A, B, C or D.

In A, the eigenvalues relative to ground are compared with experimental transition energies and comparisons improved by trial-and-error and/or least-squares techniques by iteration of the various energy parameters above. Calculation of paramagnetic susceptibilities and/or ESR g^2 tensors in route B use both eigenvalues and eigenvectors from the main diagonalization, together with one further parameter; namely, Stevens' orbital reduction factor, k , in the magnetic moment operators $\mu_\alpha = k l_\alpha + 2s_\alpha$ ($\alpha = x, y, z$). Once more, fits to available experimental quantities are converged upon by iteration of k (and, in practice, the various energy parameters also) by trial-and-error and/or least-squares methods. Within the ligand-field approach, all computations ultimately involve manipulations with matrix elements of a d orbital $|J, M_J\rangle$ basis. Routes C and D in figure 4 are discussed in sections 4.2 and 6.1.

2.6. The degree of parameterization

It is common to seek optimizations of a large number of parameters in modern ligand-field analyses. In addition to those for interelectron repulsion and spin-orbit coupling, one may consider some or all of $e_\sigma, e_{\pi x}, e_{\pi y}, e_{\pi\sigma x}, e_{\pi\sigma y}$ (the last two for misdirected valency in each of two orthogonal planes containing the M-L (z) axis), for each ligand in the complex. The number might be reduced *a priori* if, say, π bonding and/or misdirected valency for any ligation might be reasonably discounted. Further, if two ligations are diametrically opposite one another in the complex, similar types of interaction (σ and σ , or πx and πx , for example) cannot be differentiated within a single-parity basis (a consequence of the global holohedral symmetry); then a single set of parameters representing the mean contribution from the pair of ligands is employed. Finally, parameters for ligands deemed to be chemically equivalent might be made common. Even after all this, the number of independent variables is often quite large. Sometimes that number is actually greater than the apparent number of observables and one is faced with the charge of underdeterminacy. We have repeatedly found, however, that it is impossible to prejudge the determinacy in any given analysis for one or more of the following reasons: (a) constraints upon the possible behaviour of calculated ligand-field properties are imposed from the beginning by the fixed, preset molecular geometry; (b) the response of calculated properties to variation of the system

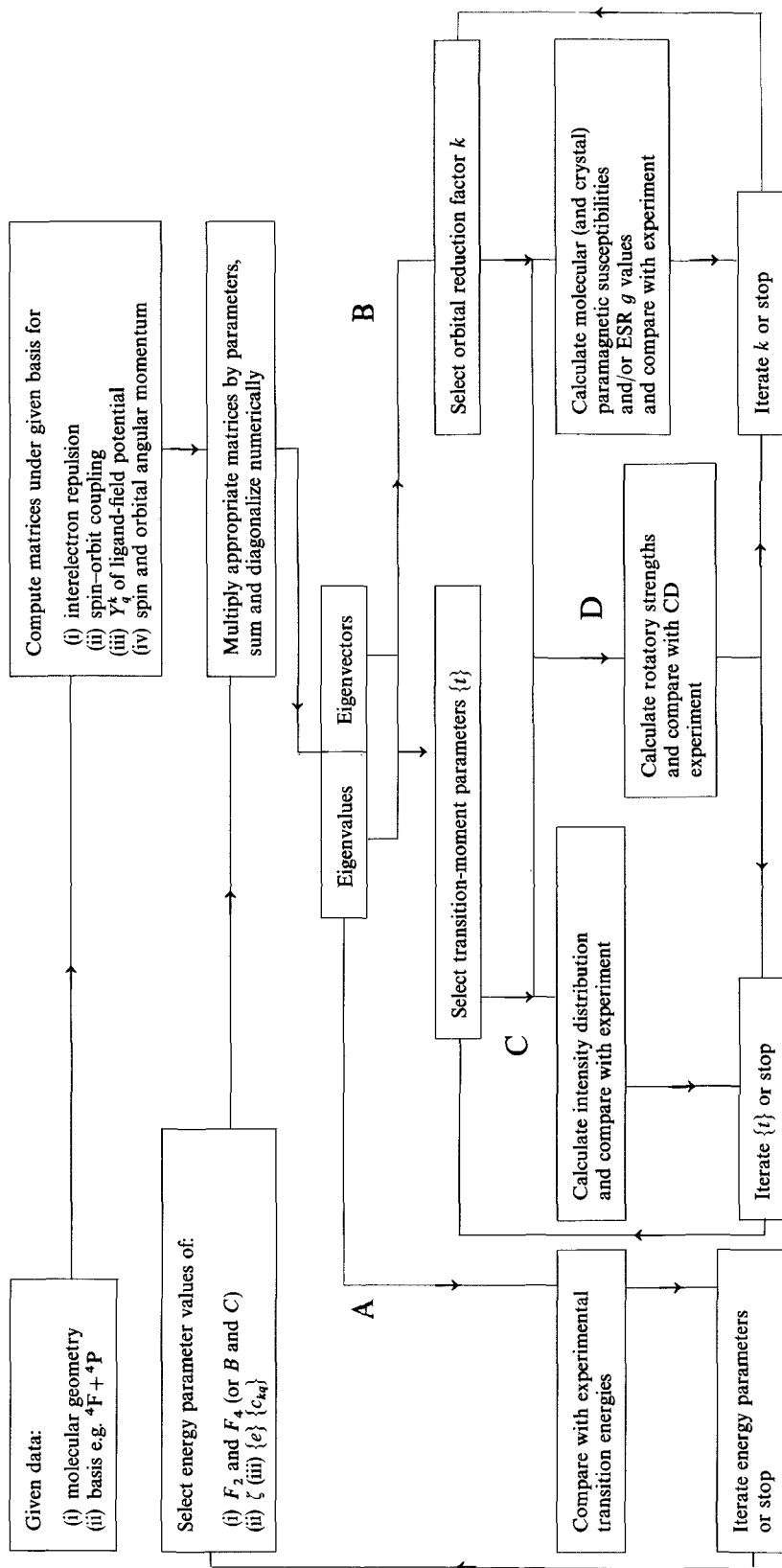


Figure 4. Block diagram of CAMMAG3 (Dale *et al.* 1989) programme indicating computational routes for (A) transition energies, (B) magnetic properties, (C) electric-dipole intensities and (D) rotatory strengths.

parameters is almost invariably nonlinear: this is sometimes large and sometimes small and, in practice, not predictable; (c) it is sometimes difficult to define the number of pieces of data offered, for example by the band energies of an optical spectrum: a 'window' or lack of optical absorbance within some energy region can be as valuable a determinant of one or more ligand-field parameters as the presence of a band itself. Faced with such intangibles, our analytical procedures are always to explore the response of the model throughout all remotely reasonable polyparameter space and so allow any actual indeterminacy to manifest itself through correlations between parameter values that afford good reproduction of experiment. Clearly it is most desirable to find singular regions of parameter space yielding good fit: and that very often occurs. Sometimes, however, two or more fitting parameters are correlated within some, perhaps wide, bounds. If so, we learn something with confidence but other things only within limits: partial success is better than no success at all. This empirical approach is not to everyone's taste but, provided the findings—good, bad and indifferent—are reported fully, there can be no legitimate complaint. In each of the ligand-field analyses reviewed in this article, that sort of detail has been reported. So also have error estimates of the various parameter values as representing bounds outside of which fits are unsatisfactory. These important details are omitted from the present review only so as not to obscure the main conclusions that have flowed from a long series of studies.

The examples presented here have addressed the ligand-field effects of misdirected valency. They have necessarily involved an increase in the degree of parameterization relative to a neglect of such effects. In order to be convinced that what has been studied here is real, we have, so far as possible, first completed analyses omitting the $e_{\pi\sigma}$ (and, if appropriate, the associated $e_{\pi x}$) parameter which fails to reproduce experiment. Only then have these extra parameters been included and shown to account for the observed properties. Though obvious, it is worth pointing out that the neglect of a parameter is tantamount to an assumption that its value is to be fixed at zero. Given the confidence borne of the many such analyses now completed, one can argue that the presumption of a fixed non-zero value for $e_{\pi\sigma}$, for example, even in systems unable to support that degree of parameterization, may be more sensible than its complete neglect.

3. Examples I: transition energies and magnetic properties

3.1. Planar low-spin cobalt(II) complexes

Planar-coordinated, low-spin complexes of cobalt(II) with a wide variety of Schiff-base ligands have long held interest as agents for reversible oxygen uptake. Studies of bulk paramagnetic susceptibilities and, especially, of electron spin resonance (ESR) g values have been reported for many and reviewed extensively by Daul *et al.* (1979). Most fall into two broad classes, corresponding to donor atom sets O_2N_2 and $N_2N'_2$, as illustrated in figure 5. Complexes in these two groups are further differentiated by the senses of the anisotropies of their ESR g^2 and susceptibility tensors. Within the common global frames of figure 5, $g_x \gg g_z > g_y$ for the CoO_2N_2 species and $g_y \gg g_z > g_x$ for the $CoN_2N'_2$ ones. A recent detailed ligand-field study (Deeth *et al.* 1987a) of one member of each coordination type has addressed these differences.

Some details of the coordination geometries of $Co(salen)$ and $Co(clamben)$ are summarized in figure 6. Single-crystal ESR spectroscopy has established the g^2 tensor in the salen complex with principal directions lying close to the approximate diads in the complex: $g_x = 3.81$, $g_z = 1.74$ and $g_y = 1.66$. In addition, the optical absorption spectrum has been reported in the range 3500 to 25000 cm^{-1} . For the clamben

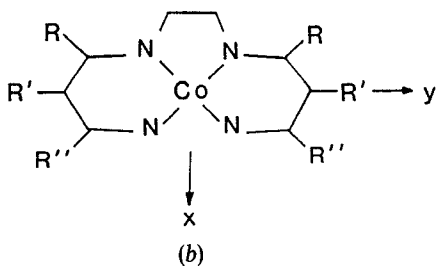
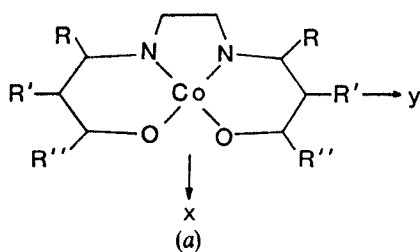


Figure 5. The structures of (a) CoO_2N_2 and (b) CoN_2N_2 species. Typical values of the anisotropies in g^2 tensors are for (a), $g_x=3.3-3.8$; $g_y=1.5-1.9$; $g_z=1.6-2.0$, $g_x \gg g_z > g_y$; and for (b), $g_x=1.75-1.95$; $g_y=2.6-2.8$; $g_z=1.8-2.0$, $g_y \gg g_z > g_x$.

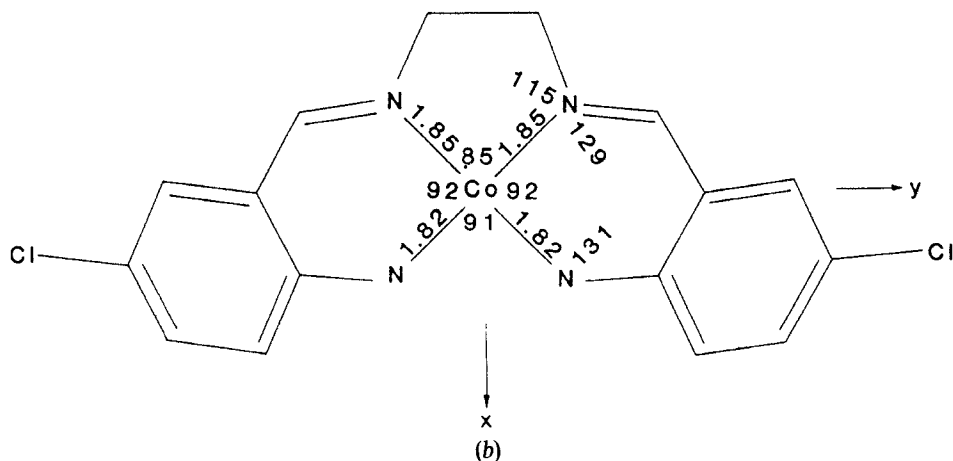
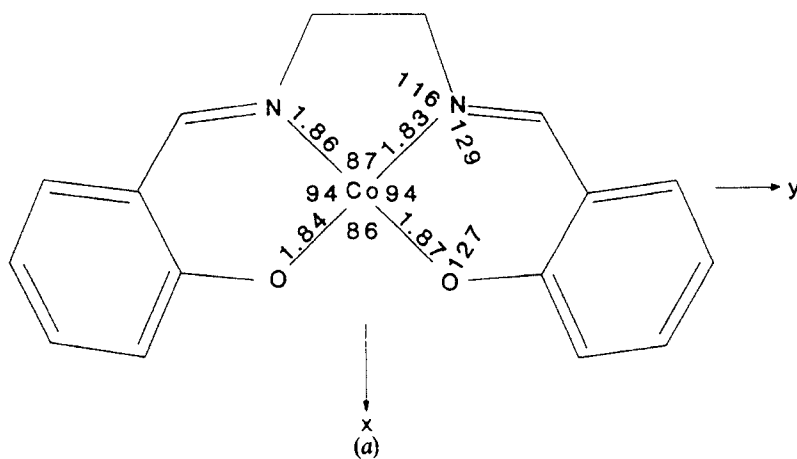


Figure 6. Coordination geometries in (a) $\text{Co}(\text{salen})$ and (b) $\text{Co}(\text{clamben})$.

complex, ESR study of a powdered sample yielded the values $g_y = 2.67$, $g_x = 2.01$, $g_z = 1.98$, the labelling being established from a single-crystal study of the paramagnetic bulk susceptibility. An electronic absorption spectrum once more completes the data base.

Ligand-field analyses for both complexes have been performed within the full d^7 configuration basis using the procedures outlined in the preceding section. In common with experience of some earlier analyses (Falvello and Gerloch 1981) of other planar, low-spin cobalt(II) complexes, the sensitivities of both magnetic and spectroscopic properties to circumstances not too far removed from spin cross-over are great. The ensuing disadvantage of difficult searches of parameter space was repaid in full by the ultimate essential uniqueness of the parameter sets affording quantitative reproduction of all observed ligand-field properties.

The analyses were initially parameterized with F_2 and F_4 for interelectron repulsion, ζ for spin-orbit coupling, and e_σ , $e_{\pi\perp}$ and e_σ (void) for the cellular ligand field. The e_σ value monitors σ bonding for the Co-N ligations in the clamben complex, or for the mean of Co-N and Co-O ligations in Co(salen); contributions from the virtually diametrically opposite ligations in the salen complex cannot be differentiated, of course. The regions above and below the coordination plane are parameterized with e_σ (void), as reviewed briefly in section 2.3. For both systems, the magnetic moment operator is parameterized with the orbital reduction factor, k , as usual. Quantitative reproductions of the spectral transition energies, ESR g^2 tensor, and of the paramagnetic susceptibility anisotropy were readily achieved for the clamben complex within this model. On the other hand, no choice whatever of these parameter values leads to the observed sense of anisotropy in the g^2 tensor of Co(salen). It is important to emphasize that the 'normal' type of analysis failed utterly.

The question arises, therefore, about what part of the ligand-field potential, and hence of the electron density close to the metal atom, is inadequately represented by the foregoing parameterization. Given the obvious difference in donor sets between clamben ($N_2N'_2$) and salen (N_2O_2), it was natural to consider the possible ligand-field role of the oxygen lone pairs. It would be disingenuous to claim that the analysis actually advanced in this way for these systems were selected from the beginning as possible candidates for a demonstration of misdirected valency. Indeed, the idea was born of an observation several years earlier (Cruse and Gerloch 1977) made during an analysis of the paramagnetic susceptibilities of a pseudo-tetrahedral nickel(II) complex involving an analogous N_2O_2 Schiff base ligator. It was established there that experiment could only be reproduced if a non-zero value of $e_{\pi\parallel}$ (that is, in the plane of Schiff base chelate) was included for the oxygen ligation but not for the nitrogen. This was ascribed to the influence of the lone pair on the oxygen.

Accordingly, the CLF parameter set for Co(salen) was enlarged to include $e_{\pi\sigma\parallel}(O)$ and $e_{\pi\parallel}(O)$ to represent any locally misdirected valency in the Co-O ligations. Ultimately, excellent reproduction of all available magnetic and spectroscopic data was achieved in this way, and with essentially unique parameter values. Optimal parameter sets for both complexes are listed in table 1. In passing, it is of interest to note the greatly reduced values of F_2 and F_4 which, as discussed in the original paper, are comprehensible through the operation of the electroneutrality principle on both metal and ligand, in conjunction with the large values of e_σ , the negative values of $e_{\pi\perp}$, and the shorter coordination bond lengths in the low-spin complexes. For our present purposes, however, the main interest lies in the magnitudes and signs of $e_{\pi\sigma\parallel}(O)$ and $e_{\pi\parallel}(O)$.

Table 1. Parameter sets yielding optimal reproduction of observed ESR g^2 tensors and d-d transition energies.

Parameter	Co(salen)	Co(clamben)
F_2 (cm^{-1})	580	400
F_4 (cm^{-1})	90	90
ζ (cm^{-1})	210	225
k	0.73	1.00
$e_\sigma(\text{N, O})$ (cm^{-1})	7100	7500
$e_{\pi\sigma//}(\text{O})$ (cm^{-1})	2500	0
$e_\sigma(\text{void})$ (cm^{-1})	-5000	-1350
$e_{\pi\perp}(\text{N, O})$ (cm^{-1})	-420	-550
$e_{\pi//}(\text{O})$ (cm^{-1})	300	0

The local x axes selected in the analysis are directed into the chelate rings, as shown in figure 7 (a). Accordingly, the sign of $e_{\pi\sigma}$ expected for a bonding orbital or energetically low-lying lone pair situated in the negative xz quadrant is positive, as discussed in section 2.4. And that indeed is found in this ligand-field analysis. The misdirected valency is also indicated by the small positive value of $e_{\pi//}(\text{O})$: from section 2.4, it is expected to be positive for donor bonds and lone pairs however they are misplaced with respect to the local Co-O axis. In principle, it is also possible that some small degree of bent bonding exists in these complexes. The possibility, based on the chelate angles shown in figure 6, is shown in exaggerated form in figure 7 (b). If real, this bent bonding is to be expected in both complexes. However, within experimental error, there is little evidence for it in the clamben complex, with respect to $e_{\pi\sigma//}$ or $e_{\pi//}$ parameter values. Were it present, a negative contribution would be expected to $e_{\pi\sigma}$ and positive to $e_{\pi//}$. Any such small contribution in the salen complex would no doubt be subsumed within the values established by the lone pair. Overall, therefore, given the ever-present possibility of combined effects of bent bonds and lone pairs, this study of planar O_2N_2 and $\text{N}_2\text{N}'_2$ coordination appears to furnish a convincing demonstration of misdirected valency, essentially arising from the oxygen lone pairs alone.

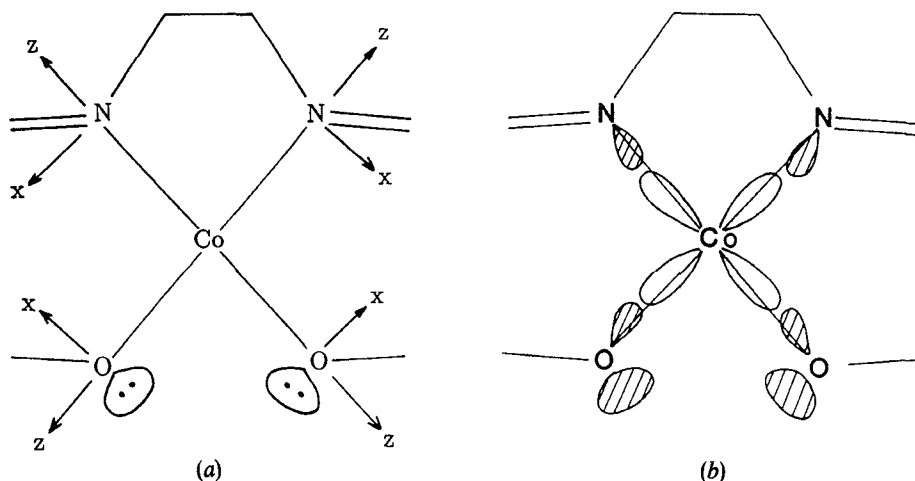


Figure 7. (a) Local reference frames in Co(salen); (b) possible bent bonding in Co(salen) or Co(clamben).

3.2. Copper acetylacetonates

Ligand-field analyses of a series of four- and five-coordinate copper(II) complexes with various substituted acetylacetonates have demonstrated (Deeth *et al.* 1987b) the role of bent bonding quite dramatically. The coordination in the MO_4 species is shown in figure 8. While copper–oxygen bond lengths, chelate ‘bite’ angles and chelate ring geometry vary insignificantly throughout the series, the angle between the acetylacetonate planes and the CoO_4 coordination planes changes markedly. The chelate rings tilt, one up, one down, so maintaining overall centrosymmetry in each chromophore. Increasing tilt angle is found empirically to be associated with increasing spectral splitting of bands at $\sim 15\,000$ and $\sim 19\,000\text{ cm}^{-1}$. In the solution spectra, only two bands are resolved for the 3-Me acac complex **1**; three for the acac, **2**, and (phenoxycarbonyl) acetonate, **3**; and four for the 3-Ph acac complex, **4**.

The key issue in the reproduction of these spectral transition energies is the splitting of the xz , yz pair of orbitals (x and y defined to lie along the copper–oxygen vectors). These d orbitals are affected by components of the ligand field operating out of the donor atom plane. Owing to the near-perfect square coordination, the energies of d_{xz} and d_{yz} are little differentiated. Trial calculations showed that, to obtain the observed splitting of $\sim 1500\text{ cm}^{-1}$ in **4**, a value for $e_{\pi\perp}(O)$ of $\sim 10\,000\text{ cm}^{-1}$ is required in

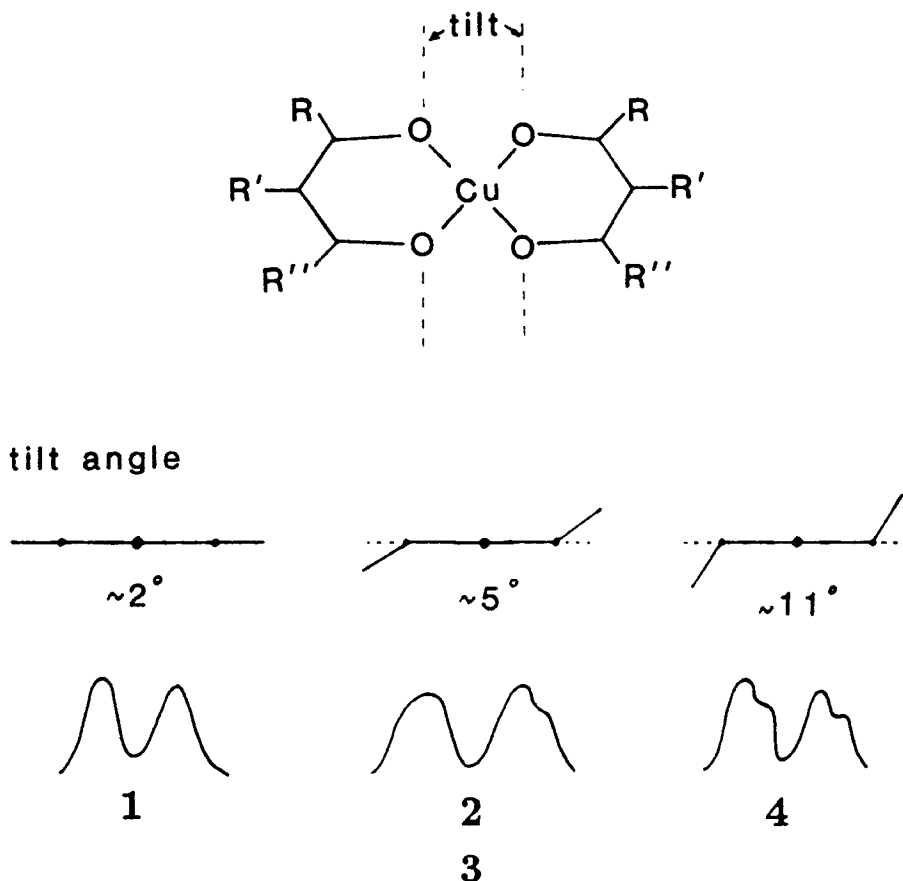


Figure 8. Coordination geometries in copper acetylacetonate species.

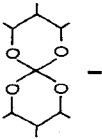
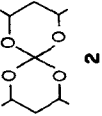
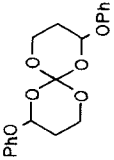
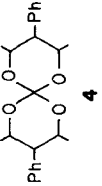
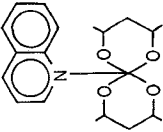
conjunction with the very slight loss of global fourfold symmetry. So, while a conventionally parameterized model is able to account for the 300 cm^{-1} splitting in **1**, it fails for the other three.

Ultimately, all transition energies throughout the series are quantitatively reproduced upon recognition of the bent bonding in the copper–oxygen ligations implied by the tilting of the acetylacetonate chelates. Optimal CLF parameter sets are given in table 2. There we observe the significant variation in $e_{\pi\sigma\perp}(\text{O})$ against an essentially constant set of all other parameters. Being based only upon the spectral transition energies, these analyses could not support totally free variation of all parameters, however. Those for $e_{\pi//}$ and $e_{\pi\sigma//}$ were held fixed throughout the series. They represent contributions arising from the non-bonding lone pairs on each oxygen atom, analogous to the situation described above for the planar cobalt species. They would not be expected to vary much with the tilt of the acetylacetonate ligands. The values determined for $e_{\pi\perp}$ throughout the series will receive contributions from the $\pi\perp$ donor function of the chelates as well as from the bent bonding, and one is unable to estimate that proportion due to the tilt. Despite these limitations, set in part by the restricted data base, the main thrust of the bent bonding being monitored by $e_{\pi\sigma\perp}$ is clear enough. The sign of $e_{\pi\sigma\perp}$ is indeterminate here for it ultimately relates to the sense of bent bonding relative to the ‘top’ of the molecule; and nothing serves to differentiate the ‘top’ from the ‘bottom’.

The sign of $e_{\pi\sigma\perp}$ has been established from an analysis of the transition energies of a five-coordinate quinoline adduct of copper(acac)₂ for, as shown in figure 9, a sense of ‘top’ is established by the overall coordination geometry. The acetylacetonate ligands again tilt about the O...O line, this time by 7° . Once more the analysis appears to be underdetermined by just four transition energies. However, spectral assignments clearly established from a polarization study by Hitchman (1974), provided a sufficiently exacting data base to establish unique values for all parameters listed in table 2. The sign of $e_{\pi\sigma//}(\text{O})$ was determined as positive, indicating the dominance of the lone-pair effect over bent bonding within the plane of the chelate: this supports the equivalent presumption in the four-coordinate species above. The much smaller value for $e_{\pi\perp}(\text{O})$ in the quinoline adduct presumably reflects a diminished ligand donor role on increasing the coordination number from four to five, in accord with the electroneutrality principle. We observe longer Cu–O bonds in the quinoline adduct in agreement with this proposal and π interactions are expected to be more sensitive to such changes than σ . The small, negative value of $e_{\sigma}(\text{ax})$ represents the sum of $e_{\sigma}(\text{N})$ and $e_{\sigma}(\text{void})$: the situation is similar to that found for the axial field in the square-pyramidal complex $[\text{Cu}(\text{NH}_3)_5]^{2+}$ (Deeth and Gerloch 1984).

As for the ligand fields arising from misdirected valency in the quinoline adduct, several views established by the preceding analysis are confirmed here. The sign of $e_{\pi\sigma\perp}(\text{O})$ is positive corresponding to the copper–oxygen bonds being displaced towards the ‘top’ of the molecule; that is, to the side of the metal coordinated by the quinoline, just as expected from the downward tilt of the acetylacetonate groups. The modest magnitude of $e_{\pi\sigma\perp}(\text{O})$ fits reasonably well with the intermediate 7° tilt of the chelates as compared with those observed in the four-coordinate acac series. Finally, the comparable values of $e_{\pi\sigma//}(\text{O})$ and $e_{\pi//}(\text{O})$ do not appear simply to reflect experimental error or model tolerances. They suggest, rather, that some contribution to $e_{\pi\sigma//}(\text{O})$ arises from bent bonding in the chelate rings themselves, as shown in figure 7(b) for the cobalt species, so diminishing $e_{\pi\sigma//}$, because the bonds would be displaced a little *into* the chelate rings, while augmenting $e_{\pi//}(\text{O})$, because the sense of displacement of bent

Table 2. Copper(II) acetylacetonate species: optimal parameter values (cm^{-1}) reproducing transition energies.

					
$e_a(\text{O})$	6000		5700	6000	5800
$e_{\pi} // (\text{O})$	100		100	100	400
$e_{\pi \perp} (\text{O})$	1200		1300	1200	200
$e_{\pi} // (\text{O})$	400		400	400	100
$e_{\text{reg} \perp} (\text{O})$	0		± 1100	± 1400	+400
$e_a(\text{ax})^\dagger$	-3600		-3100	-3300	-100
tilt \ddagger angle $^\circ$	1.8		4.2	11.4	7.0
			5.0		

† For the four-coordinate molecules, $e_a(\text{ax}) \pm e_a(\text{void})$: for the quinoline adduct, $e_a(\text{ax}) = e_a(\text{void}) + e_a(\text{N})$.

‡ Angle between the chelate and coordination planes.

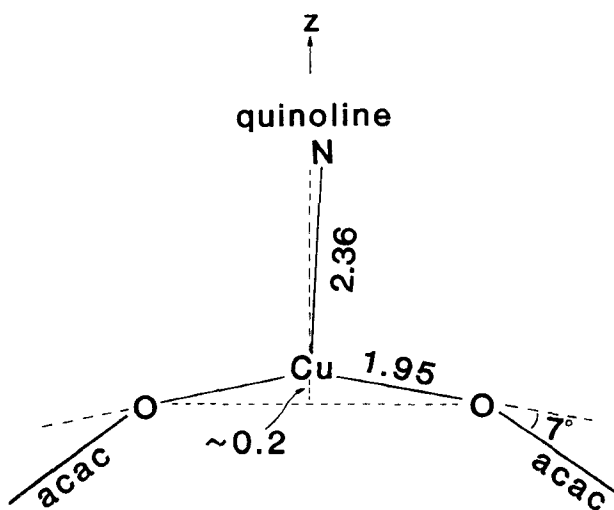


Figure 9. Coordination in $\text{Cu}(\text{acac})_2$ (quinoline).

bond or lone pair is irrelevant for this parameter. At this stage of the discussion, however, bent bonding within these chelate rings, though entirely plausible, is suggested rather than established by these analyses. Far clearer demonstrations of these effects emerge from more recent analyses and are described in section 6.2.

3.3. Lone pairs and hybridization

The validity of the ligand-field method ultimately rests on its continuing success in the reproduction of ligand-field properties with parameters that *consistently* correlate with well established chemical notions established by other means. It was disquieting, therefore, to note reports of ligand-field analyses (Bertini *et al.* 1976, Lever *et al.* 1983) on two similar nickel complexes in which thiocyanate ligands were interpreted to act as π donors in one case but as π acceptors in another. The coordination geometries of these two molecules are shown in figure 10. Reproduction of the transition energies in $\text{Ni}(\text{NH}_3)_4(\text{NCS})_2$ had been accomplished with the local ligand-field parameter values, $e_\sigma(\text{NCS}) = 3843 \text{ cm}^{-1}$ and $e_\pi(\text{NCS}) = +125 \text{ cm}^{-1}$, while those in $\text{Ni}(\text{en})_2(\text{NCS})_2$ had required the values, $e_\sigma(\text{NCS}) = 2123 \text{ cm}^{-1}$ and $e_\pi(\text{NCS}) = -409 \text{ cm}^{-1}$. The association of the smaller e_σ value in the second complex with the longer Ni-NCS bonds (2.15 *versus* 2.07 Å) has obvious appeal, but no ready explanation of the reversed π bonding role seems to be at hand. At a phenomenological level, the difference seems to be associated with the very different angles $\angle \text{Ni-N-CS}$ (180° and 140° respectively). The sum, Σ , of all locally diagonal e_λ parameters (that is, $e_\sigma + e_\pi$), equal to the trace of the molecular ligand-field matrix, for the $\text{Ni}(\text{en})_2(\text{NCS})_2$ complex is $\sim 19\,000 \text{ cm}^{-1}$. Experience of similar nominally octahedral nickel(II) complexes (Deeth and Gerloch 1987) has shown that values for the trace fall in the range 22 000 to 26 000 cm^{-1} . Reasons for the lack of a barycentre in the CLF parameterization, and hence for a non-zero trace, have been given by Woolley (1985). Elsewhere, it has been suggested that the approximate constancy for Σ , at least for a variety of ligands and coordination numbers in metal(II) species, is related to the operation of the electroneutrality

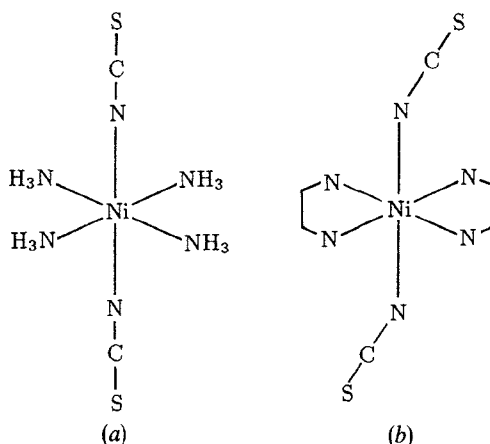


Figure 10. Coordination in (a) $\text{Ni}(\text{NH}_3)_4(\text{NCS})_2$ and (b) $\text{Ni}(\text{en})_2(\text{NCS})_2$.

principle. Whatever the reason, an approximate transferability of the trace in such ligand-field studies appears to be a useful analytical aid. The low trace in $\text{Ni}(\text{en})_2(\text{NCS})_2$ is one more reason to doubt the validity of the early analysis.

An expectation that the gross nature of the thiocyanate ligand should not vary much between these complexes does not, however, leave one oblivious of the change in hybridization that must surely accompany the change in Ni–N–CS angle. If something like an sp donor hybrid is appropriate in the linear system, an approach towards sp^2 orbitals might be presumed for the bent one. There arises, then, the possibility that the lone pair of electrons housed in the third ' sp^2 ' hybrid might make a contribution to the ligand-field energies of the metal d electrons. Alternatively, though surely less likely, one might suppose there to be no difference in hybridization of the nitrogen orbitals between the straight and bent thiocyanate ligations and hence a nickel–nitrogen bond bent by 40° . In either case, the misdirected valency should be indicated by a non-zero value for $e_{\pi\sigma}(\text{N})$ in the plane of the thiocyanate ligand. It transpires that a value of $e_{\pi\sigma}(\text{NCS})$ of $\pm 1000 \text{ cm}^{-1}$ together with $e_{\sigma}(\text{NCS}) = 2800 \text{ cm}^{-1}$ and $e_{\pi}(\text{NCS}) = +500 \text{ cm}^{-1}$, as well as sensible values for all other parameters, provides excellent reproduction of the observed transition energies, together with a value for Σ of $24\,160 \text{ cm}^{-1}$. The data base is unable to sustain a more realistic analysis in which $e_{\pi//}$ and $e_{\pi\perp}$ are differentiated though, as argued in the original paper, these values are unlikely to be very different. Overall, therefore, recognition of the misdirected valency restores the π -donor role of the thiocyanate as found in the $\text{Ni}(\text{NH}_3)_4(\text{NCS})_2$ complex, maintains the weaker σ bonding role of the more distant thiocyanate ligand, and yields a trace that is well in line with those found in many other analogous systems. *Proof* of the role of misdirected valency, in the sense that without $e_{\pi\sigma}$, reproduction of experiment is still possible, is absent in this study, in contrast to those described above. But the good sense of it is amply attested by the consistency of the other parameter values with those for related systems. In passing, we note here that the sign of $e_{\pi\sigma}$ in this study (Deeth and Gerloch 1987) is indeterminate, as in the copper acetylacetonates above, because of the lack of an independent reference in the molecule that would define it.

Another study (Fenton and Gerloch 1989a) along broadly similar lines concerns the chromophore dichlorobis(triphenylphosphine oxide)cobalt(II). In this case, however, a

more extensive data base provided by the g^2 tensor from single-crystal ESR spectroscopy together with optical transition energies from electronic solution spectroscopy does establish unambiguous ligand-field parameters for misdirected valency. The full list of optimal parameter values, obtained by analysis within the full basis of spin-quartets and doublets of d^7 , is presented in table 3: the coordination geometry is shown in figure 11. Of special interest are the values, $e_{\pi\sigma//}(\text{O}) = -100 \text{ cm}^{-1}$ and $e_{\pi//}(\text{O}) = 600 \text{ cm}^{-1}$. The small and negative value for $e_{\pi\sigma//}(\text{O})$, defined relative to the plane Co–O–P and established within 50 cm^{-1} , does not imply that the effects of misdirected valency are negligible for, otherwise, a similarly small value for $e_{\pi//}(\text{O})$ would be expected. Instead we are to see this small value of $e_{\pi\sigma//}(\text{O})$ as the net result of two contributions of opposite sign while the sources of those contributions act in concert for $e_{\pi//}(\text{O})$. The angle $\angle \text{Co–O–P}$ is about 150° . Once more, we may visualize the local bonding in the CoOP plane either to involve oxygen sp^2 hybrids together with a strongly bent bond as in figure 12(a), or as a straight bond following rehybridization of both donor and lone-pair orbitals on the oxygen, as in figure 12(b). The latter seems more likely but either viewpoint provides a ready qualitative understanding of the observed ligand-field parameters. Thus, for the situation in figure 12(a), the bent bond and lone pair lie on opposite sides of the Co–O vector and so make opposing contributions to $e_{\pi\sigma//}(\text{O})$ but additive ones to $e_{\pi//}(\text{O})$; for the case in figure 12(b), contributions to $e_{\pi\sigma//}(\text{O})$ from the two (unequal) lobes of the lone pair are opposed but, once again, those to $e_{\pi//}(\text{O})$ add. That $e_{\pi\sigma//}(\text{O})$ is observed to be negative means that the

Table 3. Optimal parameter values (cm^{-1}) for phosphine oxide, picoline-N-oxide and pyridine-N-oxide complexes.

Co(OPPh ₃) ₂ Cl ₂		[Co(OPyCH ₃) ₅](ClO ₄) ₂		[Co(OPy) ₆](ClO ₄) ₂	
$e_{\sigma}(\text{O})$	3500	$e_{\sigma}(\text{eq})$	4550	e_{σ}	3500
$e_{\pi\perp}(\text{O})$	900	$e_{\pi\perp}(\text{eq})$	400	$e_{\pi\perp}$	850
$e_{\pi//}(\text{O})$	600	$e_{\pi//}(\text{eq})$	1450	$e_{\pi//}$	450
$e_{\pi\sigma}(\text{O})$	-100	$e_{\pi\sigma}(\text{eq})$	500	$e_{\pi\sigma}$	700
$e_{\sigma}(\text{Cl})$	3350	$e_{\sigma}(\text{ax})$	4150		
$e_{\pi}(\text{Cl})$	800	$e_{\pi\perp}(\text{ax})$	75		
		$e_{\pi//}(\text{ax})$	550		
		$e_{\pi\sigma}(\text{ax})$	50		
Σ	19900	Σ	28750	Σ	28800
B	700	B	825	B	815
C^{\dagger}	2750	C^{\dagger}	3000	C^{\dagger}	3033
$k\zeta$	420	$k\zeta$	340	$k\zeta$	400

† Fixed values.

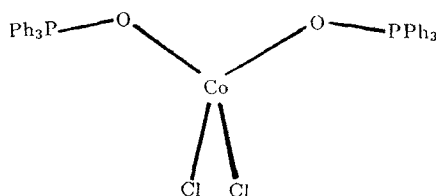


Figure 11. Coordination in Co(OPPh₃)₂Cl₂.

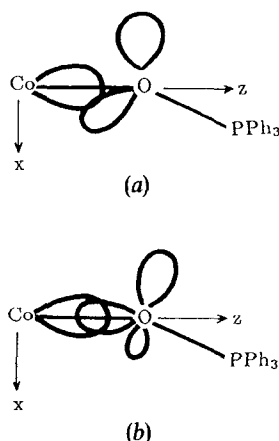


Figure 12. Two views of the Co–O bonding in $\text{Co}(\text{OPPh}_3)_2\text{Cl}_2$: (a) with formal sp^2 hybridization of the donor oxygen atom, there results bent bonding and an sp^2 lone pair in the negative xz quadrant; (b) with hybridization between sp^2 and sp , the ‘non-bonding’ lone pair of the oxygen atom possesses significant lobes in both negative and positive quadrants.

contribution from the lone-pair lobe in the positive xz quadrant is numerically the greater, despite the smaller size of that lobe, because it is much better directed towards the metal atom.

Overall, the phosphine oxides appear to act as rather poor donors in this complex. While the cobalt–oxygen bonds are not unusually long (2.00 Å), the value of $e_a(\text{O})$ in $\text{Co}(\text{OPPh}_3)_2\text{Cl}_2$ does seem rather low. The same is true of the trace, Σ , at $19\,900\text{ cm}^{-1}$. In addition to the trace values discussed above for the six-coordinate nickel(II) complexes, wide experience from ligand-field analyses of four-, five- and six-coordinate complexes of d^6 to d^9 metals in the +II oxidation state has found trace values generally in the range $21\,000$ to $25\,000\text{ cm}^{-1}$. Some variation with respect to ligand type has been observed, however: low values for complexes with phosphines, high values with imines. Reasons for these variations are not fully understood at this time though the roles of the electroneutrality principle and the nephelauxetic effect are undoubtedly relevant.

Meanwhile, further evidence of the weak donor role of the phosphine oxides in $\text{Co}(\text{OPPh}_3)_2\text{Cl}_2$ is offered by comparison between the molecular structures of this complex and its trimethylphosphine oxide analogue. The angle $\angle \text{Co–O–P}$ in the trimethyl compound is $\sim 130^\circ$ instead of the 150° in the triphenyl. This difference is not accompanied by any significant changes in Co–O or O–P bond lengths, nor in the various coordination angles about the phosphorus atom (which is essentially tetrahedral). These latter features, together with simple model building, suggest that the different $\angle \text{Co–O–P}$ angles are not the result of intramolecular packing constraints. Instead, we infer an electronic origin for the difference, reflecting the greater inductive drive of the methyl groups. These, we imagine, would increase the negative charge on the oxygen more in the trimethyl complex than in the triphenyl, so enlarging the size of the oxygen lone pairs. In turn, their greater bulk discourages the more linear Co–O–P bonding observed in the phenyl derivative. This view of the variable steric role of oxygen lone pairs, and summarized in figure 13 (a), has been exploited in the analysis of the ligand-field properties of two other, closely related, cobalt(II) complexes with oxygen ligators, as follows.

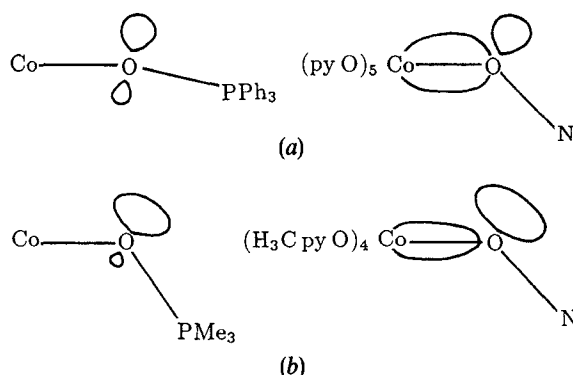


Figure 13. (a) A greater inductive drive of methyls relative to phenyls enlarges the oxygen lone pair. In turn, the greater long pair–bond pair repulsion decreases the Co–O–P angle in the methyl derivative. (b) The greater acidity of L_4Co relative to L_5Co reduces the lateral bulk of the Co–O bond so allowing a greater spread of the oxygen lone pair and increased $e_{\pi//}$ parameter in the picoline-N-oxide complex.

This study (Fenton and Gerloch 1989a) concerned the five-coordinate complex *pentakis*(picoline-N-oxide)cobalt(II) diperchlorate and the six-coordinate, *hexakis*(pyridine-N-oxide)cobalt(II)diperchlorate. Again an essentially unique set of parameter values, listed in table 3, was determined by reproduction of the wide data base in the picoline-N-oxide complex (figure 14) provided by single-crystal ESR spectroscopy together with solution electronic transmission spectroscopy: all computations were performed within the full d^7 configuration basis. Less unambiguous parameter values for the pyridine-N-oxide complex resulted from the reproduction of just the paramagnetic susceptibility anisotropy. The values presented in table 3 correspond to the selection of that set from a correlated region of polyparameter space yielding a trace value equal to that found for the picoline-N-oxide system. Any variation in this choice modifies the e values somewhat but does not change the thrust of the arguments that follow.

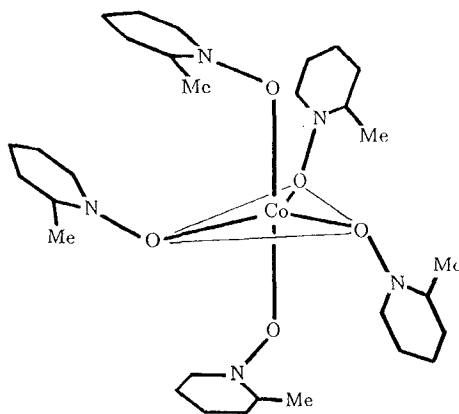


Figure 14. Coordination geometry in $[Co(O-pyCH_3)_5]^{2+}$.

The patterns of CLF e parameters found for the axial and equatorial picoline-N-oxide ligations in the five-coordinate complex are similar. The magnitudes of the parameters for the longer axial ligations are generally smaller than those for the equatorial ones, especially so for the more distance-sensitive π parameters. All of this attests the continued relevance of the ligand-field probe. Of most concern for our subject here, are the relative magnitudes of $e_{\pi//}$ and $e_{\pi\perp}$, referring to directions parallel and perpendicular to the Co–O–N planes respectively. That referring to interaction between the metal and the oxygen π donor function, $e_{\pi\perp}$, is modest while that associated with any misdirected valency in the CoON plane, $e_{\pi//}$, is large. To date, so large a value of $e_{\pi//}$ relative to $e_{\pi\perp}$ has not been observed in any other molecule. In particular it is not observed for the apparently closely related *hexakis*(pyridine-N-oxide) molecule.

It was *a priori* unlikely that picoline-N-oxide and pyridine-N-oxide offer significantly different coordination opportunities. In support of this presumption are Fenske-Hall molecular orbital calculations for the free ligands: eigenvalues and eigenvectors are as near-identical as one would expect. One feature of these calculations (Fenton and Gerloch 1989a) was particularly suggestive, however. Defining O $2p_{//}$ and O $2p_{\perp}$ as $2p$ atomic orbitals on the oxygen directed parallel and perpendicular to the heterocycle respectively, and O $2p_z$ as lying along the O–N vector, it is found that the molecular HOMO in each system comprises some 95% O $2p_{\perp}$ character while only about one electronvolt lower lies a molecular orbital with some 75% O $2p_{//}$ character. Roughly speaking, pyridine- and picoline-N-oxides offer more $2p_{\perp}$ donor function than $2p_{//}$ because the latter is somewhat engaged in bond formation with the σ framework of the heterocycle. We therefore conjecture that attack by an electrophile in the form of a transition metal will take place preferentially at the oxygen atom but in a plane perpendicular to the heterocycle rather than parallel to it. The metal–picoline-N-oxide and metal–pyridine-N-oxide ligations in the molecules illustrated in figure 14 do indeed have this geometry. The (perhaps expected) alternative in which the metal atom lies in the plane of the heterocycle so as not to compete with the heterocycle for delocalized π_{\perp} electron density is not observed in practice.

Now, in forming a σ bond with the metal, the bonding electrons will concentrate more about the line of centres (M–O) and so offer a decreased repulsion to the remaining non-bonding oxygen lone pairs. In turn, that lone-pair density will tend to move rather closer to the M–O bond-pair density. The greater the acidity of the bonded transition metal, the greater the collapse of the bond electron density and the closer the approach of the lone-pair towards the metal-oxygen bond. With this in mind, compare the prospects offered by these two complexes. In the five-coordinate complex, each picoline-N-oxide is bound to a $M(\text{picoline-N-oxide})_4$ moiety while in the six-coordinate complex, each ligand is bound to $M(\text{pyridine-N-oxide})_5$. Given that picoline-N-oxide and pyridine-N-oxide are intrinsically so similar, the acidity of the $M(\text{ligand})_4$ moiety is expected to be greater than that of the $M(\text{ligand})_5$. Thus, in the five-coordinate molecule, we expect the oxygen lone pairs to approach the metal–oxygen bond, and hence the metal itself, more closely than in the six-coordinate one. All this is summarized in figure 13(b). The larger value of $e_{\pi//}$ in the picoline-N-oxide complex than in the pyridine-N-oxide is consistent with this trend. That $e_{\pi//}$ in the five-coordinate molecule is so large anyway is to be ascribed to the non-involvement of the relevant p orbital (O $2p_{\perp}$ in the labelling scheme of the free ligand) in π bonding with the heterocycle so that the free ligand is well represented by the canonical form $C_5H_5N^+O^-$.

Finally, the smaller value for $e_{\pi//}$ in the six-coordinate complex is also attributed to the lesser acidity of the $M(\text{pyridine-N-oxide})_5$ moiety and hence decreased overall donor role of the pyridine-N-oxide itself. The large values of the ligand-field trace for these two complexes, given in table 3, presumably attest the strong σ and π donor roles of these aryl-N-oxide ligands.

4. The intensities of 'd-d' spectral bands

4.1. Early work

For decades, ligand-field studies focused exclusively upon spectral transition energies and magnetic susceptibilities. With the advent of radar, the klystron and electron spin resonance spectroscopy, g values were added to the traditional data base. A glaring omission throughout this long history was the reproduction and hence exploitation of the *intensities* of ligand-field electronic transitions. The reasons are not hard to find, for an account of electric-dipole strengths requires a description of the parity-mixing within the ligand-field 'd' orbitals. Early models considered what parity-mixing might result from configuration-mixing with terms of the lower-lying d^n manifold. Ballhausen and Liehr (1958), for example, computed the extent of mixing between 3d and 4p orbitals in free copper(II) ions and found it to be far too small to explain observed intensities of 'd-d' bands. Considerably greater success was had from a simple molecular-orbital model in which covalent mixing with ligand functions was included. Arguably the work of Judd (1962), and independently of Ofelt (1962), provided a point of departure for a great deal of effort on the intensity question during the past two decades. This concerned the absorbances in the 'f-f' transition of lanthanide complexes, the approach being to consider configuration mixing between the ground α^{f^n} and excited $\alpha^{f^{n-1}}\alpha'd'$ or $\alpha^{f^{n-1}}\alpha''g'$ configurations. A general parametric structure was developed, although it explicitly omitted any reference to the chromophore geometry. However, as Judd himself later pointed out, the *quantitative* success in the lanthanide systems had to be fortuitous in view of its neglect of important screening terms. The parametric structure of his approach, however, survives. Around the time Mason and co-workers (1975) developed an alternative view of the sources of intensity in lanthanide chromophores, though Judd (1979) provided an analytical demonstration of its equivalence with his own model. All these approaches eschewed direct mixing between f orbitals and, say, d within the ground state as the source of parity-mixing that enables electric-dipole transitions. By and large, the same appears true of the extensive work of Richardson and his colleagues (Richardson 1979, Stephens *et al.* 1984a, b, Devlin *et al.* 1987a, b) in recent years, though they might well argue that the difference between their developments of the Judd model and our own model, described shortly below, is one of parameter interpretation. No sleight is intended by the present cursory review of the development of intensity models: rather are we concerned in *this* article to focus on which recent developments in this area have contributed to the question of misdirected valency.

Although our own intensity model is equally applicable to f block chromophores, it has so far been applied exclusively to those of the d block. In it we consider electric-dipole transitions between states arising from the appropriate ground d^n configuration in which the impurity of the d orbital basis is directly parameterized. Its other major feature is its exploitation of a principle of spatial superposition, much as in the cellular ligand-field model for energies, as reviewed in section 2.3. In common with Judd's or Richardson's work, even-parity effective operators acting within a pure d basis are

constructed so that the whole computational structure falls into the ligand-field approach summarized in figure 4 and section 2.5. We confine our remarks here to an outline of the parametric structure of the model, referring those interested in the global structure and detailed formalism to the original papers (Brown *et al.* 1988a, b, c).

4.2. The parametric structure

We consider the equivalence, within each local cell, c , in the sense defined in section 2.3, between the electric-dipole operator, $e\mathbf{r}^c$ acting within a basis of cellular orbitals $\{\chi^c\}$, and an even-parity operator equivalent, $e\mathbf{T}^c$, acting within the pure d ($l=2$) basis of eigenfunctions produced by the diagonalization of \mathcal{H}_{LF} :

$$e\langle\psi_i^c|r_\alpha^c|\psi_j^c\rangle\equiv e\langle d_i^c|T_\alpha^c|d_j^c\rangle, \quad (29)$$

where $\alpha = x, y, \text{ or } z$, referred to the frame of cell c . Ultimately, the matrix elements of \mathbf{T} are expanded as a multipole series,

$$\langle d_i^c|T_\alpha^c|d_j^c\rangle = \sum_{kq} c_{kq\alpha}^c(r)\langle \hat{d}_i^c|Y_q^{(k)}|\hat{d}_j^c\rangle, \quad (30)$$

so that the usual machinery of tensor operator theory can be exploited to the full. Our focus, here, is to sketch the parameterization of the matrix elements $\langle\psi|r|\psi\rangle$ of (29) with the understanding that it provides the link between the intensity-model parameters and the expansion coefficients of (30). We begin with a view of the cellular ligand-field orbitals $\{\psi\}$.

The discussion in section 2.2 commends a view of the interactions between metal and ligands in a complex as taking place notionally in two steps. In the first, the primary bond formation in Werner-type complexes involves appropriate ligand functions together with metal s and/or p orbitals, charge redistributions and the rest. Then, we suppose the mean metal d orbitals to interact with the bond orbitals so formed. We also imagine these steps to be iterative, in the sense that d electron populations and repulsions between d electrons and bonding electrons modify the bond orbital and are then modified in their turn. ‘Traditional’ ligand-field analysis and our discussions hitherto have focused upon the differential *energy* shifts of the mean d orbitals at the end of this complex process. Here we turn our attention to the slight mixing between the mean d orbitals and the bond orbitals, writing the cellular, ligand-field orbitals as

$$\psi \sim d + b\chi. \quad (31)$$

Here d is a pure, $l=2$, ‘mean d orbital’, and χ is a composite admixed bond orbital, comprising ligand functions and metal non-d functions. For the present exposition, we simplify notation by dropping both superscripts and subscripts wherever possible. The function χ thus represents all non-d character in the cellular ligand-field orbitals from which the ‘d’ ligand-field states are built in any given, real system. As in the rest of ligand-field theory, the success of the model rests heavily upon an assumption that the description of any one ‘d’ orbital, where the quotes indicate the impurity as in (31), is satisfactorily constant throughout the manifold of ligand-field states in which they are engaged. That assumption works well for energy studies and appears to do well for intensities also. The intensity model we review here pertains only to acentric chromophores where the admixture $b\chi$ in (31) arises from the static environment and is constant in time. An extension of the model considers these admixtures to arise from the dynamic sources of molecular vibrations (Duer and Gerloch 1990). It has been

successfully applied to the reproduction and interpretation of the intensity distribution in centrosymmetric chromophores.

In order to construct a parameterization scheme for the matrix elements $\langle \psi | r | \psi \rangle$ it is convenient to express all parts of ψ relative to a common (metal) frame. This is implemented notionally by multipolar expansion of all ligand-centred parts of χ on to the metal. Altogether, for a σ type cellular orbital ψ_σ , for example, we write

$$\psi_\sigma = d_\sigma + a_1 s + a_2 p_\sigma + a_3 f_\sigma + \dots, \quad (32)$$

where all functions are now referred to the metal centre.

Electric-dipole transition moments in the local ψ basis take the form

$$\begin{aligned} \mathbf{Q} &= \langle \psi | e \mathbf{r} | \psi' \rangle \\ &= \langle d | e \mathbf{r} | d \rangle && \text{I} \\ &+ 2b \langle d | e \mathbf{r} | \chi \rangle && \text{II} \\ &+ b^2 \langle \chi | e \mathbf{r} | \chi \rangle && \text{III} \end{aligned} \quad (33)$$

The usual selection rule for electric-dipole transitions, $\Delta l = \pm 1$, means that term I vanishes and that term II survives only for those parts of χ transforming as p or f with respect to the metal centre. We define the nonzero contributions to II as *parameters* of the system:

$${}^P t_\lambda = b_p \langle d | e z | p \rangle \quad (34)$$

$${}^F t_\lambda = b_f \langle d | e z | f \rangle \quad (35)$$

$$\lambda = \sigma, \pi_x, \pi_y.$$

where the coefficients b_p and b_f subsume all earlier coefficients arising from the description of the bond orbital in (31) or of the multipole expansion coefficient in (32). For all the usual reasons relevant throughout mainstream ligand-field theory, no attempt is made to calculate such coefficients—or the radial forms of the d, p or f functions, considering, as ever, that the computation of bonding is not the proper business of ligand-field theory. The parameterization scheme outlined here merely implants the bonding and cellular structure, so effective elsewhere in ligand-field theory, into the core of the intensity procedures. Interpretations of the ${}^L t_\lambda$ parameters are then made by reference to the same qualitative chemical concepts that characterize ligand-field analyses of transition energies and magnetic properties.

The third contribution, III, to the transition moment in (33) cannot be discarded simply on the grounds that for $b \ll 1$, b^2 is negligible. For while the integrals $\langle d | e \mathbf{r} | p \rangle$ and $\langle d | e \mathbf{r} | f \rangle$ are of the order of 0.1 a.u. at most, $\langle \chi | e z | \chi \rangle$ is proportional to an effective bond length and is perhaps 10 to 20 times larger. Special circumstances of molecular geometry, however, conspire to reduce the significance of this third contribution in many cases (Brown *et al.* 1988b). Some mention of this will be made in section 5.2. Meanwhile we define the parameters

$${}^R t_\lambda = b^2 \langle \chi | e z | \chi \rangle. \quad (36)$$

from the third part of (33). Note that, throughout the definitions (34)–(36), separate parameters for transition moments parallel to x and y are not required: these quantities are related to those for ez by explicitly calculable angular integrals.

Altogether, therefore, our intensity model is parameterized at the orbital level by the local quantities ${}^L t_\lambda$; $L = P, F, R$; $\lambda = \sigma, \pi_x, \pi_y$, in much the same way that the local

Table 4. Parameters in the cellular ligand-field models.

CLF energy parameters	CLF electric-dipole transition-moment parameters
e_{σ}	$P_{t_{\sigma}}^P F_{t_{\sigma}}^F R_{t_{\sigma}}^R$
$e_{\pi x}$	$P_{t_{\pi x}}^P F_{t_{\pi x}}^F R_{t_{\pi x}}^R$
$e_{\pi y}$	$P_{t_{\pi y}}^P F_{t_{\pi y}}^F R_{t_{\pi y}}^R$

energy shifts are parameterized by e_{λ} , as summarized in table 4. Ultimately, the implementation of the present model for intensity distributions is carried out within the same general structure as for the calculation of the ligand-field properties. Route C in figure 4 shows where this fits into the scheme. Although it is possible to refine energy and intensity parameters together, we have found it easier and generally perfectly satisfactory to vary the $\{t\}$ parameter set only after the main energy diagonalization has been optimized.

Thus far, no mention of ${}^L t_{\pi\sigma}$ parameters, equivalent to $e_{\pi\sigma}$ for misdirected valency, have been discussed. In practice, they are not required. The reasons are not obvious and we shall return to the question shortly. First, however, we interrupt the present development by considering the chemical significance of the intensity parameters introduced up to this point. Although we do not provide a wide coverage of this new model for intensities in the present article, because our main attention lies elsewhere, suffice it to say that the qualitative assertions now to be introduced have already been well exemplified and continue to be supported with each new analysis. The intensity model may be relatively new but it promises to share in the general success of 'traditional' ligand-field analysis while bringing a new subtlety to that old technique.

4.3. The chemical significance of the t parameters

The right subscript in the labelling of the ${}^L t_{\lambda}$ parameters, like that in the energy e_{λ} parameters, refers to the mode of bonding being probed in the local cell and classified (for the moment) within C_{2v} pseudo-symmetry. The left superscript offers further insight into bonding than that obtained through the energy parameters. So there is a reward for the greater degree of parameterization that characterizes the intensity model. In passing, the same remarks as given in section 2.6 with regard to analytical determinacy apply within the intensity extension. Although there are inevitably more intensity variables to consider, there are also more data—especially if polarized spectra are available—and experience to date has shown that these intensity analyses tend to proceed rather more smoothly than the prior energy optimizations.

The signs of ${}^L t_{\lambda}$ parameters are expected to follow those of the corresponding e_{λ} parameters. As shown in the original paper, this expectation derives from a simple molecular orbital construction based on an assumption of weak interactions between the mean d orbitals and bond orbitals in a complex. Intensity analyses for about forty acentric transition-metal chromophores completed to date have confirmed this prediction without exception.

The magnitudes of the ${}^L t_{\lambda}$ parameters depend upon the coefficients b_p , b_f , and b in (34)–(36) and upon the integrals $\langle d|ez|p \rangle$ and $\langle d|ez|f \rangle$. The behaviours of the latter for idealized free-ion d, p, and f functions with respect to variations in bond length, metal charge and ligand charge have been explored (Brown *et al.* 1988c). They serve to

confirm the qualitative remarks below. The pre-multipliers are beyond guessing but will be small and, as with all discussions of traditional ligand-field parameters, comments must be confined to overall trends and a recognition of the smaller overlaps involved in π bonding than in σ .

In the main, the chemical significance of ${}^P t_\lambda$ and ${}^F t_\lambda$ parameter values is to be discovered from a consideration of the expansion (32). We summarize how these parameters are expected to vary with respect to bond length, bond symmetry, that is, σ versus π , and the electron distribution in a bond.

4.3.1. Bond length

Increasing separation of metal and ligand will be accompanied by decreasing metal ligand mixing, smaller b coefficients in (34) and (35), and hence decreasing magnitudes of both ${}^P t_\lambda$ and ${}^F t_\lambda$ parameters. Further, in so far that a two-centre multipole expansion reconstructs more distant ligand functions with increasing proportions of higher-order multipoles, bond lengthening is expected to diminish contributions to ${}^P t_\lambda$ parameters more rapidly than to ${}^F t_\lambda$; and so to decrease ${}^P t_\lambda : {}^F t_\lambda$ ratios. To some extent, these trends will be attenuated by the nature of the electric-dipole operator, er appearing in the integrals $\langle d|er|p \rangle$ and $\langle d|er|f \rangle$. That operator increases linearly with distance from the metal origin so that the more distant parts of relevant bond functions will contribute out of proportion to their diffuseness.

4.3.2. Bond symmetry

This last feature accounts for the fact that ${}^L t_\pi : {}^L t_\sigma$ ratios are found to be generally much larger than the corresponding $e_\pi : e_\sigma$ ratios. The energy parameters given by (13) receive their main contributions in regions close to where the acentric potential, $\mathcal{H}^{(1)}$, maximizes and are directly dependent upon the overlap between metal and ligand orbitals participating in the bond orbital. While weak π overlap, say, will diminish the appropriate b coefficients in (34) or (35), the associated electric-dipole integrals will acquire a goodly proportion of their magnitude from those parts of the π bond orbital situated near the ligand centre because of the nature of the operator er . In summary then: ${}^L t_\pi$ contributions generally appear more visible than the corresponding e_π . Now consider the dependence of ${}^P t_\sigma : {}^F t_\sigma$ and ${}^P t_\pi : {}^F t_\pi$ ratios upon bond length by reference to the two-centre expansion (26). No generality is lost if that expansion is made in terms of *one* metal-centred s orbital, *one* p_σ orbital, *one* d_σ and so on. In this form, both the expansion coefficients and the radial characters of those basis functions are varied to implement the expansion. For σ bonding, a more distant ligand function is reproduced, not only by increasing contributions from higher- l functions, but also by more expanded radial functions. So far as this effect is concerned, one need not expect any dramatic change in the ratio $\langle d|ez|p \rangle : \langle d|ez|f \rangle$, though there will be some. The main action upon ${}^P t_\sigma : {}^F t_\sigma$ ratios will arise, as discussed above, from the changing proportions of p and f functions in the expansion.

The situation is rather different for π orbital expansion, however. Greater metal–ligand separation in this case is reproduced very poorly by expansion of the radial properties of the expansion basis, for otherwise an unwanted lateral expansion of the π orbital would accompany bond stretching. Instead longer bonds give rise almost exclusively to higher- l functions of essentially unchanged radial character. Other things being equal, longer bonds will increase the $F:P$ ratio of t_π parameters much more rapidly than of t_σ parameters.

4.3.3. Electron distribution in the bonds

Qualitatively, increasing polarization of bond orbitals towards the metal is expected to affect both absolute values and the $P:F$ ratios of ${}^L t_\lambda$ parameters somewhat like bond shortening. The two variables might be considered together in terms of an 'effective bond length'. Changes in bond strength and character along some series might also affect the lateral bulk of the bonding electron density. At one extreme, for example, strong σ donation by a ligand might result in bonding electrons that concentrate strongly about the internuclear vector in order to minimize their potential energy with respect to both nuclei. At another, diffuse bonds might better minimize total energy. Consider then, some series in which the lateral bulk of an object bond increases while all else, including bond length, stays constant. Such variations would be reproduced within the expansion (32) by a greater diffuseness and enlargement of the radial factors of the expansion functions, together with a diminished role of higher- l functions so as to cancel this effect parallel to the bond vector. We would then expect to see 'fatter' bonds favour larger ${}^P t_\lambda : {}^F t_\lambda$ ratios than 'thinner' ones.

Overall, these ideas, together with older ones developed for CLF energy parameters, have served to provide a coherent overview of the results of analyses of the intensity distributions within the 'd-d' spectra in some forty transition-metal complexes. However, within the analyses to be described in this article they are involved only in so far as they clarify the question of misdirected valency. It has been important, however, to provide this summary if only to illustrate the detail and reach of the new intensity model within ligand-field analysis.

4.4. Intensity parameterization for misdirected valency

In view of the importance of the off-diagonal energy parameter, $e_{\pi\sigma}$, to the probing of misdirected valency, it is natural to enquire about any corresponding amendment of the $\{t\}$ parameter set for intensities. It has been shown (Duer and Gerloch 1989a) that quite extensive formal changes to the t parameterization scheme are required in these circumstances but reasonable arguments have been made, and tested empirically, which suggest that a satisfactory account is made just by reinterpretation of ${}^L t_\sigma$ and ${}^L t_\pi$ parameters in the plane of the misdirected valency. Here, we restrict discussion to a demonstration of, what is in practice, this more important feature.

Consider two parallel circumstances: (a) that of a well directed σ bond with no attendant π bond, and (b) that of a misdirected σ bond or non-bonding lone pair, again without any other π bond in the plane (xz) in question. For (a), the cellular orbitals are simply

$$\psi_\sigma \sim d_{z^2} + b\chi_{\sigma}, \quad (37)$$

$$\psi_\pi \sim d_{xz}. \quad (38)$$

The t parameters associated with this situation are ${}^P t_\sigma, {}^F t_\sigma$ with ${}^P t_{\pi x} = {}^F t_{\pi x} = 0$. For (b), we recognize that the bent ' σ ' bond or lone pair can be resolved into two components, ϕ_σ and $\phi_{\pi x}$, say, and so write zeroth-order cellular orbitals as

$$\psi'_\sigma \sim d_{z^2} + \beta\phi_\sigma, \quad (39)$$

$$\psi'_{\pi x} \sim d_{xz} + \beta'\phi_{\pi x}. \quad (40)$$

In the local C_2 symmetry of misdirected valence in the xz plane, these functions mix to some extent:

$$\psi''_{\sigma} \sim d_{z^2} + \beta\phi_{\sigma} + \gamma(d_{xz} + \beta'\phi_{\pi x}), \quad (41)$$

$$\psi''_{\pi x} \sim d_{xz} + \beta'\phi_{\pi x} + \gamma'(d_{z^2} + \beta\phi_{\sigma}). \quad (42)$$

This small mixing is neglected in the first-order summary given here: actual analyses so far support this tactic in practice. However, even with this neglect, the differences between (39), (40) and (37), (38) cannot be ignored. The admixture of some ligand function into d_{xz} and the decreased admixture into d_{z^2} imply non-zero ${}^L t_{\pi x}$ parameter values and modified ${}^L t_{\sigma}$. Without an experimental reference, any change to ${}^L t_{\sigma}$ values cannot be recognized. Altogether, therefore, the main indicator of misdirected valency in the intensity parameterization would be non-zero ${}^L t_{\pi x}$ values in circumstances where 'normal' πx bonding was deemed, or otherwise established, to be absent.

The sign of any ${}^L t_{\pi x}$ parameter arising from misdirected valency can be predicted by similar arguments to those used to predict signs of t parameters in C_{2v} symmetry. We do not reproduce the detailed arguments here but observe that the essential determinant of these signs is the donor or acceptor role of the ligand. In the circumstances of figure 2, for bent bonds or lone pairs, positive signs are predicted for ${}^L t_{\pi x}$ values.

5. Examples II: transition intensities

We now return to our review of analyses attesting the role of misdirected valency in coordination chemistry. The following two examples illustrate the exploitation of both e and t parameterizations in this area; in the first, with respect to experimental 'd-d' transition energies and intensities; and, in the second, with respect to the very wide data gleaned from 'd-d' energies and intensities, single-crystal paramagnetic susceptibilities and ESR g^2 tensors.

5.1. A trigonal bipyramidal nickel(II) Schiff-base complex

The coordination geometry of the complex shown in figure 15 is approximately trigonal bipyramidal. Five band maxima have been observed in the electronic spectra of single crystals of *bis*(salicylidene- γ -iminopropyl)methylaminenickel(II), abbreviated to Ni(salmedpt). Band resolution is incomplete, however, so that areas for four sufficiently discrete energy ranges in each of two polarizations provide the data base for the intensity analysis (Duer and Gerloch 1989a).

In addition to Racah B and C parameters, and a fixed spin-orbit coupling coefficient, ζ , the energy analysis comprised the CLF parameter set: $e_{\sigma}(\text{im})$, $e_{\pi \perp}(\text{im})$ for

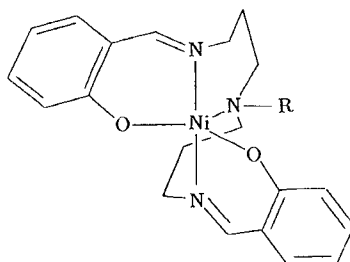


Figure 15. Coordination geometry in Ni(salmedpt).

the Schiff base imines lying at the axial sites of the trigonal bipyramids, $e_{\sigma}(\text{am})$ for the equatorial amine, e_{σ} , $e_{\pi\perp}$, $e_{\pi\parallel}$, $e_{\pi\sigma}$ for the equatorial phenolic oxygen donors (\parallel and \perp refer to directions parallel and perpendicular to the salicylidene rings). Preliminary, though extensive, calculations with $e_{\pi\parallel}(\text{O})$ and $e_{\pi\sigma}(\text{O})$ fixed at zero—that is, with neglect of any misdirected valency—signally failed to reproduce the observed transition energies. A good account of experiment was achieved, however, with free variations of all the energy variables listed above. Fits were not perfectly unique, occurring within a small, correlated region of parameter space. Typical parameter values are listed in table 5. Of particular importance for the ensuing intensity analysis, however, is the fact that the equivalent, global multipolar representation of the ligand field is essentially constant throughout the region of correlation. Thus, any small indeterminacy in the energy analysis does not carry over into the intensity analysis.

The intensity distribution in this complex is dominated by the equatorial ligands and the parameters ${}^L t_{\sigma}(\text{am})$, ${}^L t_{\sigma}(\text{O})$, ${}^L t_{\pi\parallel}(\text{O})$ and ${}^L t_{\pi\perp}(\text{O})$, for $L=P, F, R$, although contributions with $L=R$ were expected, and empirically found, to be slight because of the triangular disposition of these ligands. The near irrelevance of the axial ligands follows from the imines being situated nearly centrosymmetrically with respect to the metal. In these circumstances, the 'static' intensity model correctly finds their contributions to cancel, or very nearly so. The main departure from this centric symmetry lies in the inexact parallelism of the N=C bonds. We have therefore omitted ${}^L t_{\sigma}(\text{im})$ parameters from the analysis and only included ${}^L t_{\pi\perp}(\text{im})$ towards the end of the process, but these too were found to be unimportant in practice. After extensive trial-and-error exploration of parameter space, followed by least squared refinement, the observed intensity distribution within eight bands (four for each of two polarizations) was reproduced quantitatively and essentially uniquely. The corresponding t parameter set is included in table 5. The quality of both energy and intensity fits is illustrated in figure 16. Reproduction of the intensities is also given numerically in table 6. Included in that table is a comparison between simultaneously computed average (unpolarized) intensities and those obtained separately from a solution experiment: these latter data formed no part of the analytical process.

We comment upon the optimal e and t parameter sets of table 5 under four headings.

Table 5. Optimal energy and intensity parameters for Ni(salmedpt).

Energy parameter	Value (cm^{-1})	Intensity parameter	Value†
$e_{\sigma}(\text{am})$	3300	${}^P t_{\sigma}(\text{am})$	100
		${}^F t_{\sigma}(\text{am})$	64
$e_{\sigma}(\text{O})$	4000	${}^P t_{\sigma}(\text{O})$	0
		${}^F t_{\sigma}(\text{O})$	53
$e_{\pi\perp}(\text{O})$	1100	${}^P t_{\pi\perp}(\text{O})$	45
		${}^F t_{\pi\perp}(\text{O})$	8
$e_{\pi\parallel}(\text{O})$	25	${}^P t_{\pi\parallel}(\text{O})$	61
		${}^F t_{\pi\parallel}(\text{O})$	2
$e_{\pi\sigma}(\text{O})$	1200		
$e_{\sigma}(\text{im})$	5100		
$e_{\pi\perp}(\text{im})$	0		

† Arbitrary units.

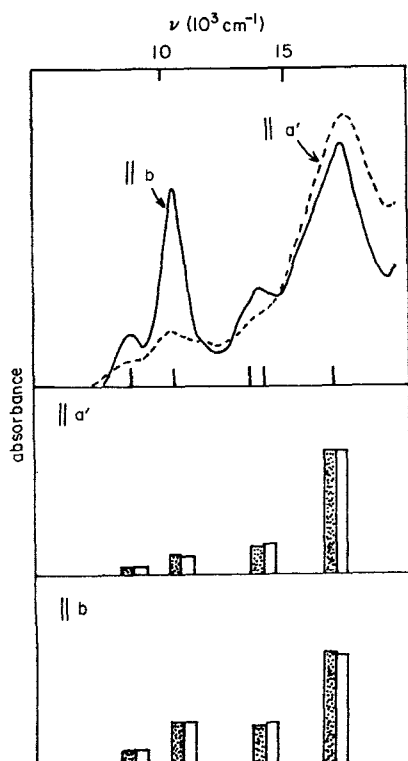


Figure 16. Polarized spectrum of Ni(salmedpt). Optimal calculated transition energies are shown by vertical markers. Histograms display observed (dark) and calculated intensity distributions. See also table 5.

Table 6. Comparison between observed relative† intensities and those calculated with the parameter sets of table 5 for Ni(salmedpt).

Energy range (cm^{-1})	Polarization a'		Polarization b		Average‡	
	Obs.	Calc.	Obs.	Calc.	Obs.	Calc.
8000–9200	2	2	3	3	24	9
9500–11 000	5	4	11	11		
12 000–14 700	7	8	10	11	76	34
14 700–18 000	33	33	30	29		

† All intensities are expressed as percentages of the total areas in the spectra observed either for crystals or for solutions.

‡ Average intensities are from the solution spectrum and from the means of calculated intensities for light polarized $//a'$, $//b$, $//c$.

5.1.1. 'Non-bonding' oxygen lone pairs

The positive sign found for $e_{\pi\sigma}(\text{O})$ corresponds to an off-axis perturbation of the Ni–O ligation situated outside the Schiff-base chelate rings and is thus compatible with the role of the oxygen lone pair. The misdirected valency is also evidenced strongly by the relative magnitude of the ${}^P t_{\pi//}(\text{O})$ intensity parameter. (Note, in passing, that in the absence of absolute experimental intensities, the t parameters in table 5 are given on an arbitrary scale only.) That the P contribution so overwhelms the F is not to be understood in terms of a strong polarization towards the metal but rather of a relatively wide lateral spread of the lone pair that would accord with its expected diffuseness. Further, the important role of the off-axis perturbation for intensities, as compared with energies, is to be seen as a manifestation of the way the electric-dipole operator emphasizes those parts of the local environment which are more distant from the metal, as discussed in section 4.3.

5.1.2. M–L σ bonding

The e_{σ} parameters indicate M–L σ bonding decreasing along the series imine > oxygen > amine. The much larger value for the imine ligation is quite typical of the axial fields found in other trigonal bipyramidal complexes of nickel(II) and copper(II). It arises from the greater d electron density in the equatorial plane relative to that along the principal axis, together with the demands of the electroneutrality principle. Analogous forces act in the square-pyramidal complexes described in the following section. The larger σ fields of the phenolic oxygen ligations relative to that of the amine, on the other hand, presumably reflect a greater electron donation from the formally negatively charged oxygen donor. As that charge leaves the oxygen atom it concentrates more strongly about the internuclear axis. The relative compactness of the Ni–O bond over the Ni–amine is monitored by the greater ${}^F t_{\sigma} : {}^P t_{\sigma}$ ratio in the former, as determined by the intensity analysis. Similar qualities characterize the Co–O and Co–N bonds in studies of CoO_2S_2 and CoN_2S_2 chromophores (Duer and Gerloch 1989b).

5.1.3. Ni–O π_{\perp} bonding

The Schiff-base oxygens act as both σ and π donors. The smaller ratio ${}^P t_{\pi\perp}(\text{O}) : {}^F t_{\pi\perp}(\text{O})$ relative to ${}^P t_{\pi//}(\text{O}) : {}^F t_{\pi//}(\text{O})$ suggests that the 'normal' π bond orbital is laterally less diffuse than the lone pair.

5.1.4. Ni–imine π_{\perp} bonding

Both energy and intensity analyses define a negligible π donor role for the axial imine groups. This appears to be a consequence of the steric role of the d shell. First, the d_{xz} and d_{yz} orbitals (referred to z as the 'threefold' axis of the trigonal bipyramidal coordination) are full and so tend to oppose π donation from the axial ligands. Secondly, and probably more important, is that the d configuration that facilitated strong axial σ donation inevitably frustrates π donation from the same ligands because of their tendency to achieve electroneutrality.

5.2. Square-pyramidal arsine oxide complexes of cobalt(II) and nickel(II)

The complexes $\text{M}(\text{Ph}_2\text{MeAsO})_4$; $\text{M} = \text{Co(II)}, \text{Ni(II)}$; $\text{X} = \text{NO}_3^-, \text{ClO}_4^-$ comprise anions X together with cations $[\text{M}(\text{Ph}_2\text{MeAsO})_4\text{X}]^+$ possessing approximate square-based pyramidal geometry. The complex ions lie on a crystallographic tetrad in the

solid but cannot, of course, possess fourfold symmetry. The original X-ray structure determination, published only in preliminary form (Pauling *et al.* 1965) suggested that these ions occupied the fourfold sites statistically. A recent and complete structural analysis of $[\text{Ni}(\text{Ph}_2\text{MeAsO})_4\text{NO}_3]^+\text{NO}_3^-$ confirms that (Falvello *et al.* 1987). The sketch of the complex coordination geometry in figure 17 shows a fourfold disposition of the basal arsine oxides together with an axial nitrate ligand arranged in an unsymmetrical way in any one molecule.

Measurements of ligand-field properties over the years have covered a wide range. These systems illustrate the power of ligand-field analysis more comprehensively, perhaps, than any other system reported to date. A full description of these studies

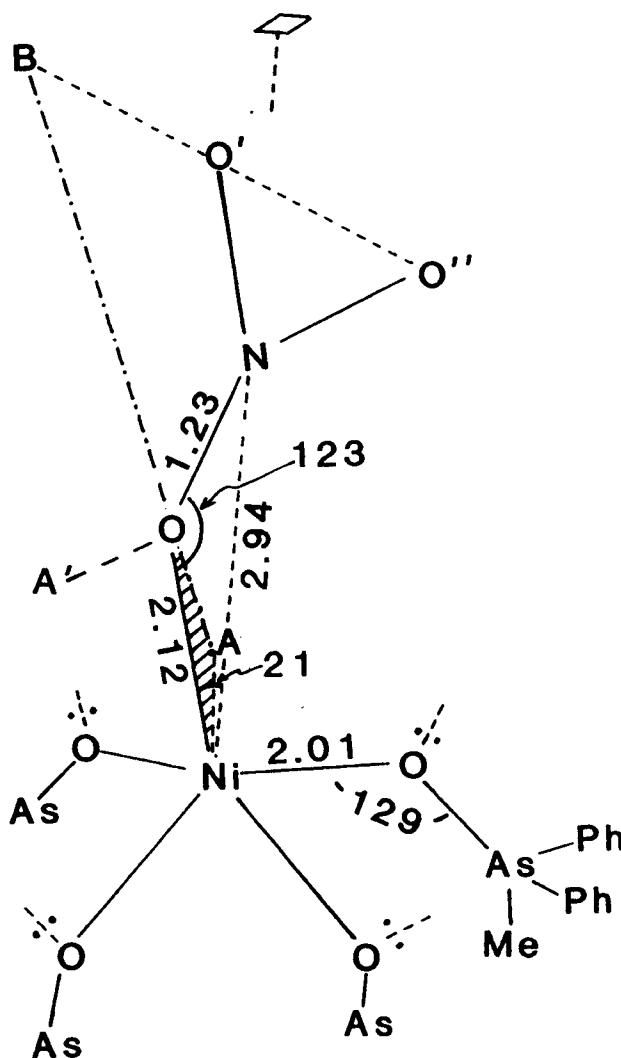


Figure 17. Coordination in $[\text{Ni}(\text{OAsPh}_2\text{Me})_4\text{NO}_3]^+$. OA and OA' represent the directions of oxygen sp^2 lone pairs in the plane of the nitrate ligand. AO meets O'O' at B in the same plane. AB is the line of intersection of planes NiAO and the nitrate group. O'O'' and O'B are of equal length.

would be far too long and detailed within the present article: while brief mention of most aspects of both experiment and analysis will be made, our remarks emphasize those features particularly relevant to the misdirected valency question. For both nickel and cobalt arsine oxide complexes with nitrate, single-crystal polarized optical spectra at various temperatures between 20 and 300 K have been recorded. Single-crystal paramagnetic susceptibilities for both have been measured in the temperature range 80 to 300 K. These are all *crystal* properties and so properly labelled parallel and perpendicular to the unique crystal axis in the tetragonal space group. More recently, Bencini *et al.* (1979) reported a careful study of the single-crystal ESR g^2 tensor in the d^7 cobalt complex. That recorded the *molecular* property and reflected the less-than-fourfold symmetry of the molecules in the lattice. The data provided by this study comprised not only the magnitudes of the principal molecular g values but also their all-important orientations. We summarize a 'traditional' ligand-field analysis (Fenton and Gerloch 1987) which sought to reproduce all these data quantitatively and then sketch a subsequent analysis (Fenton and Gerloch 1989b) of the intensity distributions observed in the optical 'd-d' spectra.

5.2.1. Analyses

Both arsine oxide and nitrate ligations were candidates for misdirected valency. The interactions with the arsine oxides were expected to resemble those with the phosphine oxides described in section 3.3. That with the axial nitrate, however, is a little more subtle. Experimentally, the anisotropy of the molecular g^2 tensor in the plane roughly normal to the crystal c axis is enormous ($g_1 = 8.6, g_2 = 1.3$). Since this anisotropy must arise from the non-axial nature of the $M-ONO_2$ bonding, it is important to identify a local $M-NO_3$ coordinate frame that best reflects the likely local bonding. This was done by initially assuming sp^2 hybridization of the donor oxygen orbitals. The vectors OA and OA' in figure 17 are coplanar with the nitrate plane and equilaterally disposed with respect to the ON vector. The metal-nitrate ligation is non-ideal in two respects, (a) because the σ bonding oxygen lobe along OA is not directed exactly at the metal atom, and (b) because the metal atom lies some 0.38 \AA out of the NO_3 plane. The local reference frame for the nitrate ligation was chosen with z taken along the $M-O$ vector, as usual, and y taken perpendicular to the plane MOA : positive x was chosen to lie on the same side of the $M-O$ bond as A . This construction ultimately depends only upon the presumed triangular hybridization of the donor oxygen atom. Any inadequacy in that assumption would lead ultimately to a better choice of local frame being one rotated somewhat with respect to the above. The possibility was checked empirically in the full analysis with the conclusion that the frame chosen initially was optimal within two or three degrees.

In addition to the usual interelectron repulsion parameters (B and C for the full d^7 or d^8 bases ultimately employed) and the spin-orbit coupling coefficient, ζ , the ligand-field Hamiltonian was parameterized with the CLF set: $e_\sigma, e_{\pi\perp}, e_{\pi\parallel}, e_{\pi\sigma\parallel}$ for each ligation type, namely arsine oxide and nitrate. Only the reproduction of the widely extensive data enabled values for all members of this large parameter set to be established. For the cobalt complex, the combination of the orientation of the g^2 tensor and the crystal susceptibilities proved to be the most demanding data and determinant of the ultimate parameter set. For the nickel system, reproduction of the optical transition energies turned out to be the most exacting task. The analyses were difficult and time-consuming but did establish virtually unique sets of parameter values yielding quantitative reproduction of *all* data. Small areas of correlation between best-fit

parameters were found but nothing of what follows is substantially altered by taking alternative fits within those regions. The optimized parameter sets are given in table 7 and the quality of fit shown in figure 18 and in tables 8 and 9.

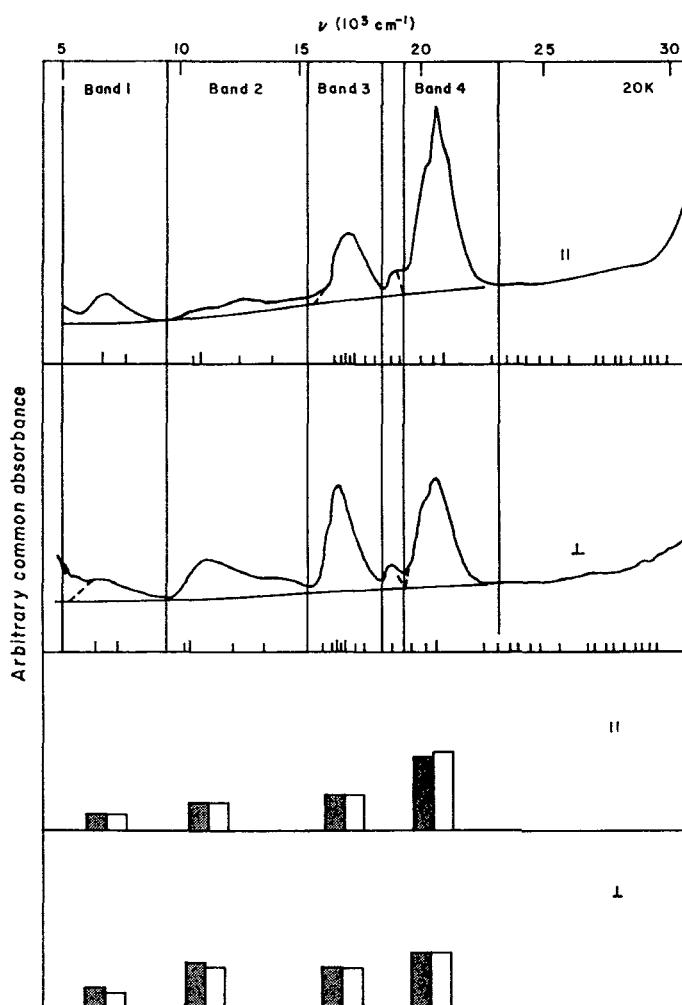
The intensity analysis was based upon the relative intensities of the spectra shown in figure 18. The parameter set comprized L_{t_σ} , $L_{t_{\pi//}}$ and $L_{t_{\pi\perp}}$ with $L = P, F$ and R for both arsine oxide and nitrate ligations. Similar analyses were conducted independently for the nickel and cobalt chromophores. Initially, variations of only P and F type parameters were investigated. They identified regions of good reproduction of all intensities whose response to variations in the R type parameters were then studied. The reasons for this two-stage process are as follows. For any one ligation, the main R -type contribution by far relates to the electric dipole oriented parallel to the M-L (z) axis. The sum of such contributions over all ligations in a complex is given by $\sum_i q_i^R \cos \theta_i$ where each R -type local transition moment q_i^R is oriented parallel to a bond vector inclined at an angle θ_i to the arbitrary but fixed global z axis. It is simple to show that such sums vanish in the global molecular symmetries of bipyramids and antiprisms. There is some tendency for similar cancellation in the present square-based pyramids. The basal ligands are oriented at about 101° to the formal molecular tetrad, so that the axial contribution from the nitrate R terms will cancel those from the four basal arsine oxides when ${}^R t_{\lambda}(\text{NO}_3) \sim 0.73 {}^R t_{\lambda}(\text{AsO})$. As discussed below, the energy and magnetism analyses just described established weaker interactions between metal and nitrate than between metal and arsine oxide; and the Ni-ONO₂ and Ni-O (arsine oxide) bond lengths are 2.01 and 2.12 Å respectively. Although there are further differences between the axial ligations of the cobalt and nickel chromophores, described shortly, it was expected that overall R contributions would be small and ${}^R t_{\lambda}$ parameters not well defined. The second steps of the intensity analyses considered variations of $\Delta^R t_{\lambda}$, being the differences between arsine oxide and nitrate R -type contributions. Little correlation between the model's response to these ΔR contributions and to P and F contributions was observed. Ultimately, excellent and essentially unique reproduction of the experimental intensity distributions in these chromophores was achieved with the parameter sets listed in table 10. The quality of fit for the spin-allowed bands is shown in figure 18. In passing, we record that similarly good reproduction of the relative intensities within the spin-forbidden bands was also achieved, though these data were not included in the analytical process. It is also of interest to note that a simplistic computation (Fenton and Gerloch 1989b) of relative band widths provided a good account of experiment also.

Table 7. CLF e parameters (cm^{-1}) affording optimal reproduction of crystal paramagnetic susceptibilities, molecular g^2 tensor (for the cobalt complex) and d-d transition energies in $[\text{M}(\text{OAsPh}_2\text{Me})_4\text{NO}_3]^+\text{NO}_3^-$.

CLF e Parameter	M = cobalt (II)		M = nickel (II)	
	Arsine oxide	Nitrate	Arsine oxide	Nitrate
e_σ	3500	100	3550	1700
$e_{\pi\perp}$	980	-200	950	100
$e_{\pi//}$	875	650	675	350
$e_{\pi\sigma}$	945	950	880	1650

Table 8. Comparison between the observed and calculated g^2 tensor in $[\text{Co}(\text{OAsPh}_2\text{Me})_4\text{NO}_3]\text{NO}_3$.

	Observed				Calculated		
	Orientation relative to				Orientation relative to		
	<i>a</i>	<i>b</i>	<i>c</i>		<i>a</i>	<i>b</i>	<i>c</i>
$g_1 = 8.6$	90	11.5	77.5	$g_1 = 8.59$	90	11	79
$g_2 = 1.3$	0	90	0	$g_2 = 1.29$	1	90	89
$g_3 = 0.91$	90	77.5	168.5	$g_3 = 0.93$	89	79	169



(a)

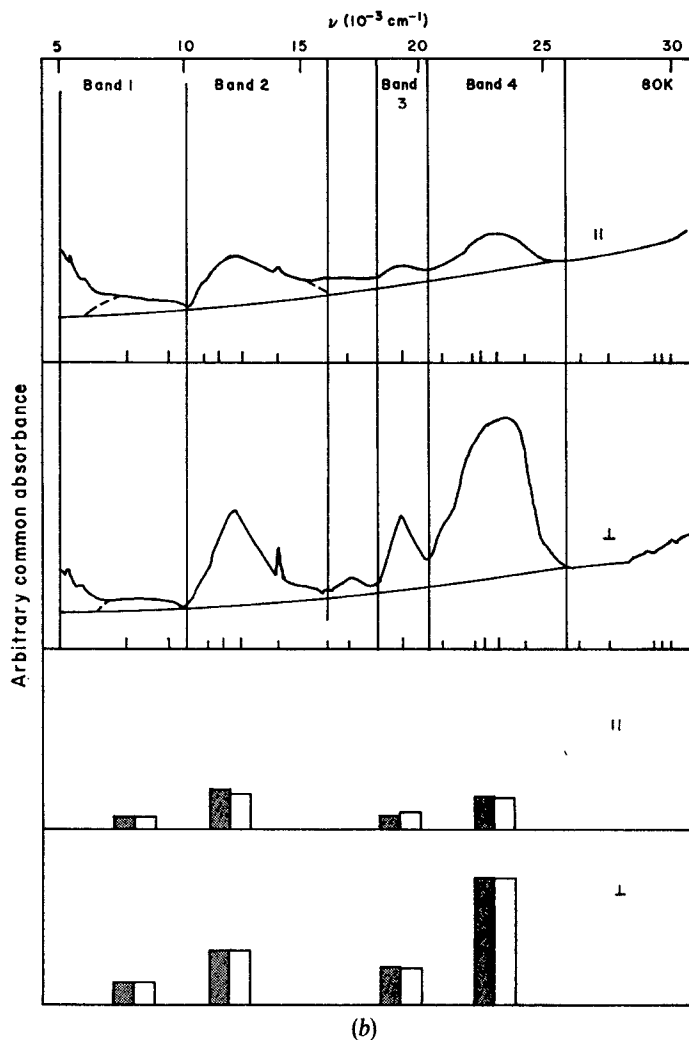


Figure 18. Polarized spectra for $[M(\text{OAsPh}_2\text{Me})_4\text{NO}_3]^+\text{NO}_3^-$; (a), $M=\text{Co}$, (b), $M=\text{Ni}$. Optimally calculated transition energies are indicated by long markers for spin-allowed transitions and by short markers for spin-forbidden. Histograms display observed (dark) and calculated intensity distributions.

Table 9. Comparisons between observed and calculated crystal susceptibilities† ($\chi/\text{c.g.s.u.} \times 10^{-4}$) for $[M(\text{OAsPh}_2\text{Me})_4\text{NO}_3]\text{NO}_3$.

Temperature (K)	M = cobalt(II)				M = nickel(II)			
	χ_{\parallel}		χ_{\perp}		χ_{\parallel}		χ_{\perp}	
	Obs.	Calc.	Obs.	Calc.	Obs.	Calc.	Obs.	Calc.
300	65	62	128	135	40	40	52	52
200	86	81	194	204	59	58	77	78
140	96	98	283	295	80	80	111	110
100	108	113	395	413	105	106	156	155

† Defined parallel (\parallel) and perpendicular (\perp) to the tetragonal crystal c axes.

Table 10. Intensity parameters† reproducing observed intensity distributions in the spin-allowed optical spectrum of $[M(\text{OAsPh}_2\text{Me})_4\text{NO}_3]^+(\text{NO}_3)^-$.

CLF t parameter	M = cobalt(II)		M = nickel(II)	
	Arsine oxide	Nitrate	Arsine oxide	Nitrate
$P t_\sigma$	100	0	100	15
$F t_\sigma$	20	0	20	50
$P t_{\pi\perp}$	20	0	25	0
$F t_{\pi\perp}$	70	-20	85	0
$P t_{\pi\parallel}$	35	0	35	0
$F t_{\pi\parallel}$	0	10	0	10
$\Delta^R t_\lambda = {}^R t_\lambda(\text{AsO}) - {}^R t_\lambda(\text{NO}_3)$				
$\Delta^R t_\sigma$	10		0	
$\Delta^R t_{\pi\perp}$	10		-10	
$\Delta^R t_{\pi\parallel}$	0		0	

† Arbitrary units: values given relative to $P t_\sigma(\text{AsO}) \approx 100$ for each chromophore.

5.2.2. Results

In reviewing the optimal e and t parameter sets listed in tables 7 and 10, we focus on just two points in this article: the difference between the axial ligations in the cobalt and nickel species, and the details relating to misdirected valency. The most obvious difference between the parameter sets of the cobalt and nickel systems is that shown by the $e_\sigma(\text{NO}_3)$ values (100 and 1700 cm^{-1} respectively). These energies represent the sums of e_σ values for nitrate and the coordination void sited diametrically opposite. From a recent study of the ligand-field roles of coordination voids, a reasonable estimate for $e_\sigma(\text{void})$ here is -2500 cm^{-1} so that 'corrected' values for $e_\sigma(\text{NO}_3)$ are in the region 2600 and 4200 cm^{-1} for the cobalt and nickel species respectively. We address the difference between these values. Increasing effective nuclear charge of nickel(II) compared with cobalt(II) is expected to be accompanied by some bond shortening and increased ligand-field strength. Such changes will not occur isotropically, however, at least because of the changing asymmetry in the repulsive role of the partly filled d shell. The ordering of the d orbitals in these square-pyramidal complexes is expected to be $E(d_{x^2-y^2}) > E(d_{z^2})$ and $E(d_{xy}) > E(d_{xz}, d_{yz})$. In the strong-field limit, the change cobalt \rightarrow nickel is accompanied by the configurational change

$$(xz, yz)^4(xy)^1(z^2)^1(x^2 - y^2)^1 \rightarrow (xz, yz)^4(xy)^2(z^2)^1(x^2 - y^2)^1$$

and hence by increased d shell repulsion in the basal plane. The greater Lewis acidity of the nickel atom should then be satisfied more easily by shortening of the axial ligation and accompanied by an increased $e_\sigma(\text{axial})$ value, as observed. The t parameters in table 10 independently confirm this view. On average, ${}^L t_\sigma(\text{NO}_3)$ values are less than ${}^L t_\sigma(\text{AsO})$ ones, but particularly so for the cobalt chromophore. We also note the dominance of the F contributions over the P for the axial σ bonding (to be contrasted with the situation for the arsine oxide ligation) indicating a long effective bond length, which again agrees with the structural details of figure 17. The weaker nitrate coordination in the cobalt complex is also supported by the ΔR contributions in table 10.

The patterns of both e and t parameters in these complexes provide interesting commentary on each type of misdirected valency discussed here. The ligand fields of both ligand types in both complexes are characterized by substantial values for $e_{\pi\sigma}$. The positive signs for $e_{\pi\sigma}(\text{AsO})$ correlate with misdirected valence density sited on the same side of the M–O (arsine oxide) bond as the non-bonding oxygen lone pairs. As \angle MOR angles commonly exceed 120° and relatively unhindered, if small, reorientations of the non-chelating arsine oxide ligands about the metals appear possible, we presume that M–O bonding overlap has been maximized and that bent bonding is minimal. The non-zero $e_{\pi\sigma}(\text{AsO})$ values thus appear to monitor the ligand-field effects of the lone pairs.

Bent bonding does seem likely, however, in the metal–nitrate interactions because the metal atom does not lie in the ligand plane. The ligation appears to reveal a compromise between intramolecular bonding forces, which are weak, and intermolecular crystal forces. Further, the choice of local axes discussed above is such that the positive $e_{\pi\sigma}(\text{NO}_3)$ value is to be correlated with misdirected valence density situated on the opposite side to the oxygen non-bonding lone pair. In short, the ligand-field effects of bent bonding (positive $e_{\pi\sigma}$) overwhelm those of the lone pair (negative $e_{\pi\sigma}$).

The intensity parameters in table 10 accord with the views of electron distribution built from the e parameters. The typically short M–OAs bonds (2.01 \AA) are associated with ${}^P t_\sigma > {}^F t_\sigma$. That ${}^F t_{\pi\perp} > {}^P t_{\pi\perp}$, on the other hand, is to be understood in terms of the general tendency for t_π parameters to be dominated by F contributions, as outlined in section 4.3. Then what of the fact that ${}^P t_{\pi\parallel} \gg {}^F t_{\pi\parallel}$? This result appears to be a splendid confirmation of the misdirected valency established by the ‘energy’ analysis. As discussed in section 4.4, ${}^L t_{\pi\parallel}$ contributions arise here from the misdirected valency ‘scrambling’ ${}^L t_\sigma$ and ${}^L t_{\pi\parallel}$ values. In effect, the ${}^L t_{\pi\parallel}$ parameter acquires some of the character of ${}^L t_\sigma$. We note that, for both ligand types in both chromophores, the relative magnitudes of ${}^P t_{\pi\parallel}$ and ${}^F t_{\pi\parallel}$ mirror those of the corresponding ${}^P t_\sigma$ and ${}^F t_\sigma$ parameter. In particular, for the long Ni–ONO₂ bonds (2.12 \AA), F type contributions to intensity dominate P type as expected. Also, because of the way the electric-dipole operator emphasizes more distant parts of a bond orbital, ${}^F t_{\pi\parallel}(\text{NO}_3)$ values are far from negligible in either chromophore.

5.2.3. Summary

It has not been possible to give more than an outline of these extensive and detailed analyses. Their inclusion has been to show that the ideas developed in earlier sections continue to apply and that interpretations of intensity parameters (which is still a relatively new art) qualitatively support those made by reference to the e parameters from transition energies and magnetism. In the final sections, we describe studies of circular dichroism in which evidence of bent bonding relies as heavily on the t parameterization as on the e . On embarking upon this story, it is good to know that analyses of the electric-dipole transitions in some forty disparate chromophores, all of which have involved prior e type parameterizations, consistently confirm and illuminate the detailed views of electron density distributions established by the more traditional methods.

6. Examples III: exploitation of circular dichroism

6.1. The computational route

A chiral molecule is one lacking improper rotation symmetry; it absorbs left and right circularly polarized light differentially. The circular dichroism (CD) experiment

measures this differential absorption, $\Delta\varepsilon = \varepsilon_L - \varepsilon_R$, a quantity related to the so-called rotatory strength. The theory of CD is well understood but not reproduced here. It is sufficient for our present purposes to note that the rotatory strength for a transition $i \rightarrow j$ in an optically active (chiral) solution, for example, is proportional to the scalar product of the electric- and magnetic-dipole transition moments. For the CD of 'd-d' transitions, we already have a model and computational procedures available within our ligand-field approach. Electric-dipole transition moments are represented parametrically *via* the t variables and magnetic-dipole moments *via* the operators $\mu_\alpha = kl_\alpha + 2s_\alpha$ ($\alpha = x, y, z$), and the orbital reduction factor, k . Within the CAMMAG3 system, route D in figure 4 provides the means of calculating and refining circular dichroism. We emphasize that these calculations, like those of absorption intensities, transition energies, magnetic susceptibilities and ESR g^2 tensors, are all performed within the d ($l=2$) ligand-field basis. Interpretations of experimental 'd-d' circular dichroism (as opposed, say, to the CD associated with charge-transfer or ligand spectra) are therefore to be made by reference to the first coordination shell in the first instance. In the examples which follow, analyses of CD are intimately linked with analyses of absorbance strengths and of all other available ligand-field properties. Results emerge numerically from the computational package and there has been no need to apply general 'simplifying' concepts such as sector rules. The reproduction of the magnitudes and signs of experimental CD spectra automatically means that a proper description of molecular optical handedness is made.

6.2. Bent bonding in chiral four- and five-coordinate chromophores

Two recent studies describe the first application of the cellular ligand-field model to the quantitative reproduction and interpretation of the circular dichroism observed in eleven transition-metal complexes. One (Fenton and Gerloch 1990a) concerned three nominally tetrahedral cobalt(II) molecules; the other (Fenton and Gerloch 1990b) eight formally trigonal bipyramidal complexes of cobalt(II) and nickel(II). Their coordination geometries are shown in figures 19 and 20.

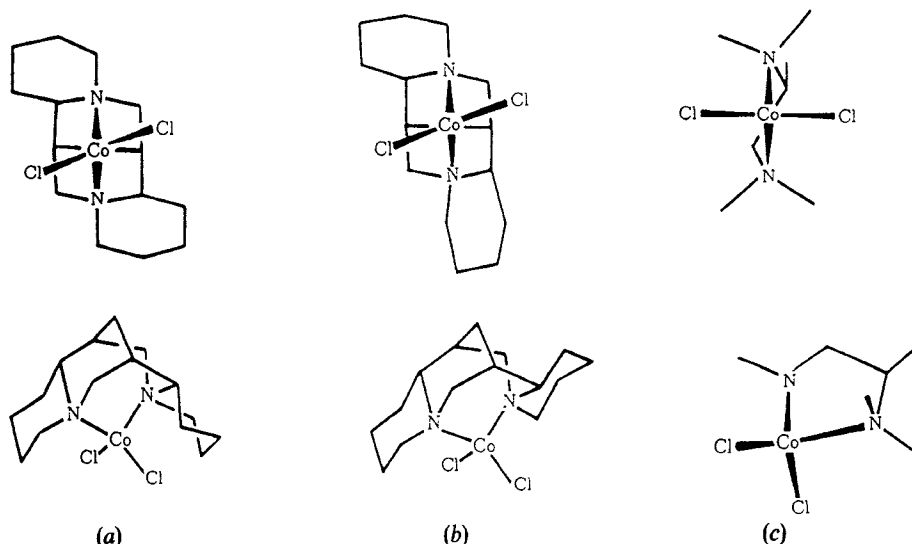


Figure 19. Coordination geometries of CoN_2Cl_2 species: (a) with the α -isosparteine ligand, (b) with sparteine, (c) with the tetramethylpropylenediamine ligand.

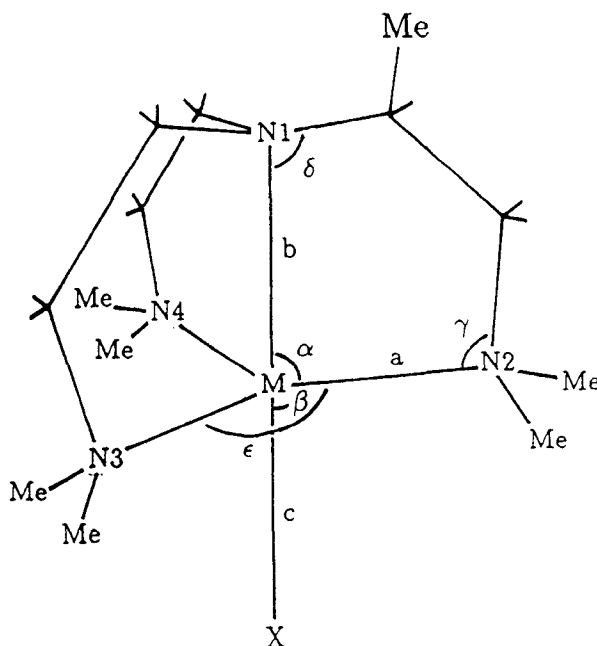


Figure 20. Coordination geometry for $[M(S\text{-tan})X]^+$ species; $M = \text{Co(II)}, \text{Ni(II)}$; $X = \text{NCS}, \text{Cl}, \text{Br}, \text{I}$.

For each series, ligand-field analysis sought to reproduce experimental 'd-d' transition energies, absorbances and rotatory strengths obtained from solution studies. Absorption and circular dichroism data for the sparteine complexes in figure 21 were particularly extensive and detailed, covering the frequency range 2000 to 20 000 cm^{-1} .

From the beginning, the source of chirality in the two sparteine molecules was seen as the relative twisting of the ClCoCl and NCoN' planes caused by steric interference between the chlorine atoms and the rigid, bulky sparteines. One should note, however, that the twisting is considerably greater in the α -isoparteine system, in which steric hindrance is doubly effective, than in the sparteine but the magnitudes of the observed circular dichroism in the two chromophores are roughly similar. About the same CD magnitude was observed for the propylenediamine complex though here the ClCoCl and NCoN' planes are nearly exactly normal to each other. Obviously the structural chirality in the propylenediamine chain is ultimately responsible for the optical activity in this system but the d orbitals can only recognize this within the first coordination shell which, as just noted, is essentially achiral. A similar problem applies for the origin of optical chirality in the trigonal bipyramidal species in figure 20. The tripod ligand, S-tan, takes on a $\delta\delta\delta$ conformation and so provides the ultimate source of optical activity in these systems. Nevertheless, the disposition of donor atoms about the central metal in each complex very nearly possesses mirror symmetry. Once again, the question arises as to how the chiral conformation of the ligand communicates itself to the metal d orbitals via an essentially achiral first coordination shell.

In the first stage of analysis, the ligand fields in all these complexes were represented by what might be called the 'basic' parameter set; that is, e_σ only for all amines plus e_σ and e_π for all halogens. Perfectly satisfactory reproductions of transition energies were

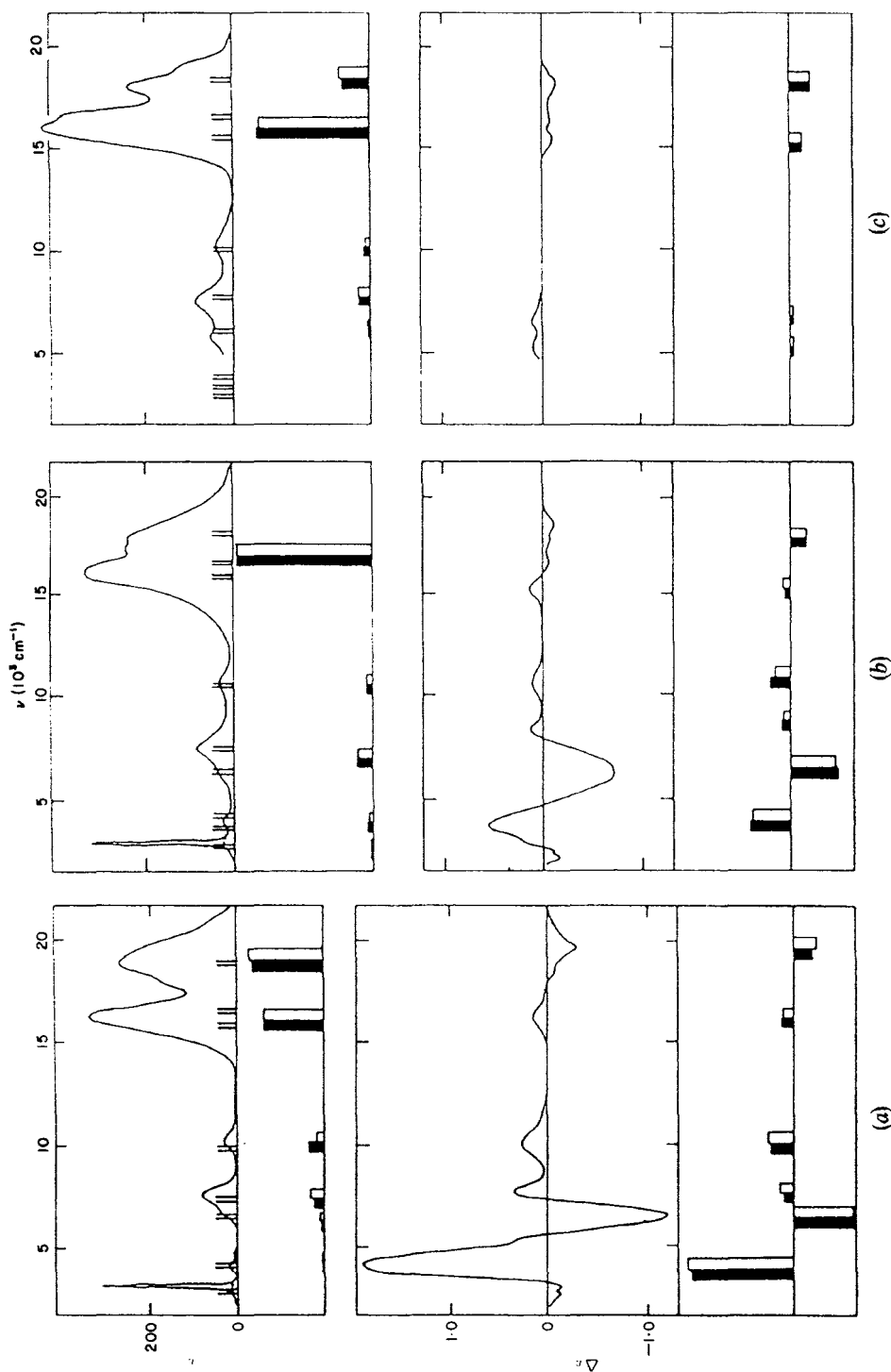


Figure 21. Absorption and circular dichroism spectra of the CoN_2Cl_2 species, (a) α -isosparteine, (b) sparteine and (c) propylenediamine complexes. Optimal calculated transition energies are indicated by vertical markers. Histograms display observed (dark) and calculated intensities (e) or CD ($\Delta\epsilon$). See also table 11.

obtained in this way for each chromophore in each series. Then, within analyses of intensities, a 'basic' set of t parameters was considered, comprising ${}^L t_\sigma$ for amines and ${}^L t_\sigma$ plus ${}^L t_\pi$ for halogens. Once again, good accounts of all observed absorbances were obtained after suitable explorations of parameter space. Had there been no data beyond the absorption spectra, the analyses would have been concluded at this stage. Reproduction of the CD rotatory strengths, on the other hand, failed dramatically in each case. The only extra variable in the CD calculations is the orbital reduction factor k in the magnetic moment operator. The magnitude of calculated rotatory strengths is roughly proportional to k , because contributions from the spin angular momentum operator are very small (arising only out of spin-orbit coupling effects). In all these analyses, we sought to reproduce experiment with k values in the usual range (as known from many susceptibility and ESR g value studies) of 0.7 to 1.0. Apart from this small degree of flexibility, the e and t parameter sets that optimize reproduction of transition energies and intensities automatically determine rotatory strengths. For the two sparteine chromophores, the calculated rotatory strengths were found to be an order of magnitude too large, although the patterns of signs for the various transitions, shown in figure 21, were reproduced reasonably well. By contrast, the calculated rotatory strengths for the propylenediamine (figure 21) and for the eight trigonal bipyramidal complexes, shown in figure 22, were an order of magnitude too small: for the latter complexes, the sign patterns were not reproduced either.

A popular response to these failures might well be to remind us that we seek to reproduce solution properties using molecular geometries determined in the solid state. This is, of course, the spectroscopic equivalent of the argument used by some crystallographers that all structural anomalies are due to 'crystal packing effects'. As ever, the problem with this line of argument is to prove it wrong. Some attempt was made to do just that, however, by calculating rotatory strengths as a function of small geometry changes. For the α -sparteine system, for example, reasonable good reproduction of the observed CD can be achieved if the angle between the ClCoCl' and NCoN' planes is reduced from the observed 19° to about 1° . There seems to be no good reason to believe in a geometry change of that sort of magnitude caused by solvent effects: further, the transition energies are well represented within the *four*-coordinate model. For a wide variety of ligand-field studies involving many different properties, analyses have consistently been completed successfully without recourse to putative structural changes on dissolution. So, our ligand-field analyses in the present case were restarted with a reconsideration of the ligand-field description rather than of geometry variation.

Consider first the sparteine molecules. While the ClCoCl angle is very close to the ideal tetrahedral 109° in each chromophore, the NCoN' angle is $\sim 90^\circ$. This small angle is quite usual, of course, within an ethylenediamine-like chelate but it does suggest a compromise between the demands of the cobalt atom to be tetrahedral and of the ring to be closed. Recalling the arguments of section 1, we take the view that close to the metal atom, the electron density associated with four bond pairs tends to be arranged tetrahedrally so as to minimize interelectron repulsion energies: the disposition of the chlorine ligands, which are free to move, support this. A similar disposition of electron density close to the donor nitrogen atoms is to be expected for the same reason. In between the metal and donor atoms, a compromise is reached and bent bonds result. The proposition was tested within the present ligand-field analyses by inclusion into the parameter sets of all monitors of misdirected valency in the planes defined by N, Co, N'; namely, $e_{\pi\sigma//}(\text{N})$, $e_{\pi//}(\text{N})$ and ${}^L t_{\pi//}(\text{N})$. After small concomitant variations in all other

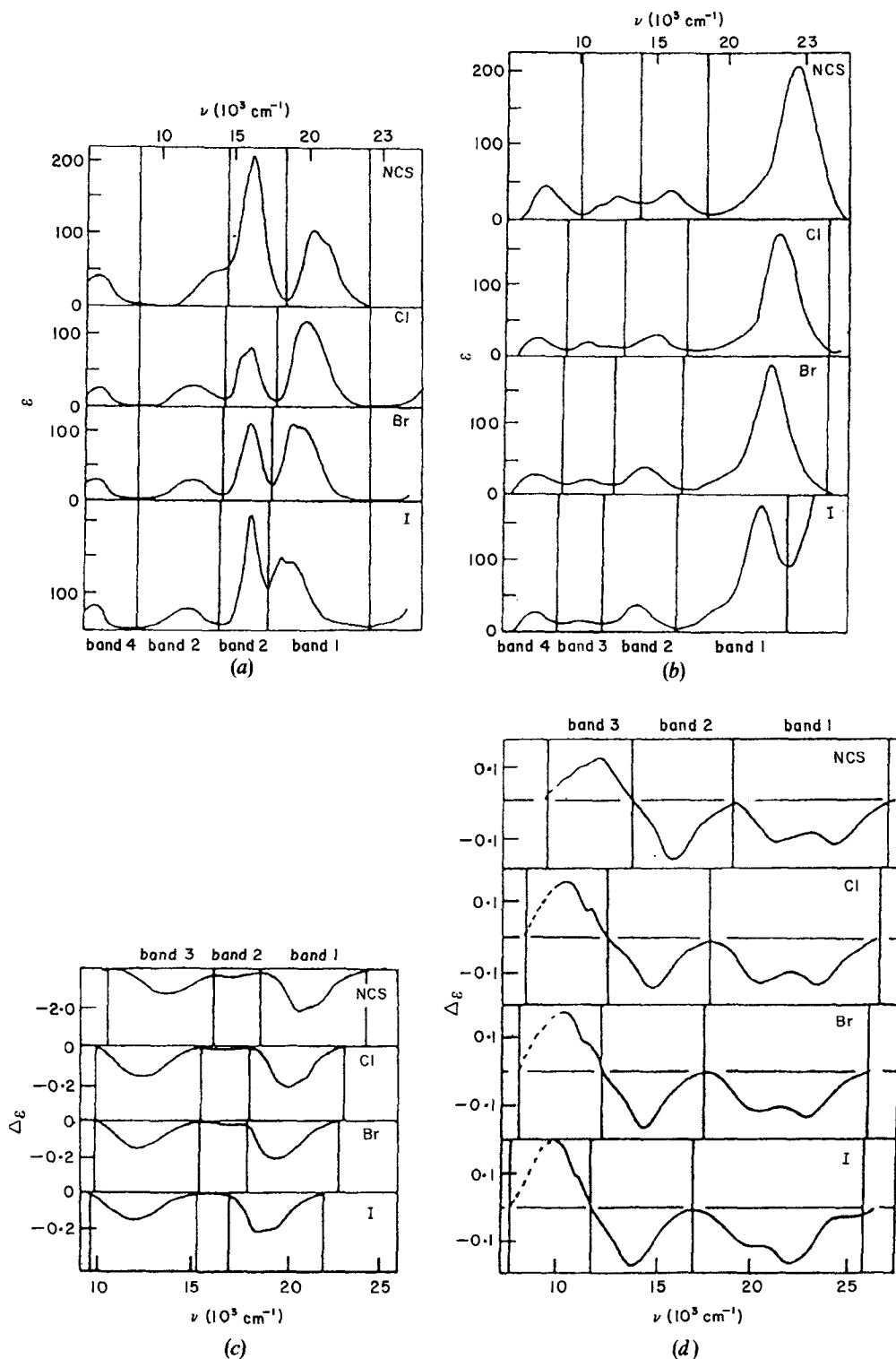


Figure 22. Absorption (a) for $[\text{Co}(\text{S-tan})\text{X}]^+$ and (b) for $[\text{Ni}(\text{S-tan})\text{X}]^+$ species. CD spectra for (c) Co species, and (d) Ni species.

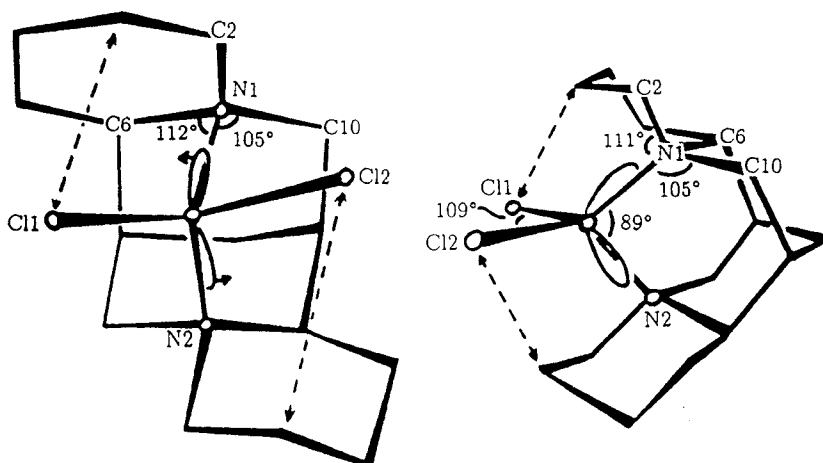


Figure 23. Proposed bent bonding in the sparteine complexes.

parameters, good reproductions of both transition energies and intensities were restored. The agreement between calculated and observed rotatory strengths was improved somewhat but was nevertheless quite unsatisfactory; a factor of about five times too large rather than eleven times. We therefore reconsidered our modelling of the misdirected valency once again.

If one pursues the view of bond electron density distributions being compromises between overlap in the central bond region and interelectron repulsion forces closer to the atomic centres, one must recognize the incompleteness of the parametric structure described thus far. The ClCoCl' plane is rotated from the normal to the NCoN' plane because of the steric interactions between chlorines and the sparteine ligand. So, if the electronic distribution about, and near to, the cobalt atom is essentially tetrahedral, the bent Co-N bonds are displaced not only wider than the $\angle \text{N-Co-N}$ angle but also to the side, as sketched in figure 23. In other words, the chirality probed by the metal d orbitals is of a lesser magnitude than suggested by the first coordination shell. This immediately implies a lesser optical activity and rotatory strength. The idea was implemented within the ligand-field model by inclusion of $e_{\pi\sigma\perp}$, $e_{\pi\perp}$ and ${}^L t_{\pi\perp}$ parameters for the cobalt-amine ligations normal to the NCoN' plane. After wide-ranging exploration of the now large parameter space, excellent reproduction of *all* experimental properties was achieved. With so large a degree of parameterization, however, it is not surprising to find that good-fit parameter values are extensively correlated. Within the correlated region, however, some clear conclusions could be made: (a) representatives of *both* senses of bent bonding (\parallel and \perp) are required and non-zero values of both e and t parameters are necessary. (This is entirely satisfactory, for the physical view of the bent bonding offered here is not consistent unless the effects of both chelation and twisting are included); (b) that $e_{\pi\sigma}$ values of the order 500 cm^{-1} are needed; and (c) that the values of the 'basic', $e_{\sigma}(\text{N})$, $e_{\sigma}(\text{Cl})$, and $e_{\pi}(\text{Cl})$, parameters are not grossly modified by inclusion of those concerned with misdirected valency. This last point means that the analysis of circular dichroism served to refine and illuminate, rather than invalidate, the earlier analyses of transition energies and intensities alone. For illustrative purposes, we list a representative optimal parameter set for the 'tetrahedral' chromophores in table 11 and show the corresponding quality of reproduction of both absorbances and rotatory strengths in figure 21.

Table 11. Parameter sets affording quantitative reproduction of 'd-d' transition energies, spectral absorbance and rotatory strengths in CoN_2Cl_2 .

Parameter	Sparteine	α -Isosparteine	Propylenediamine
$e_\sigma(\text{Cl})^\dagger$	4000	4100	3800
$e_\pi(\text{Cl})$	1300	1300	1100
$e_\sigma(\text{N})$	4800	5000	4250
$e_{\pi//}(\text{N})$	20	75	75
$e_{\pi\sigma//}(\text{N})$	-400	-300	-250
$e_{\pi\perp}(\text{N})$	180	150	300
$e_{\pi\sigma\perp}(\text{N})$	+100	+200	-300
B	750	750	720
ζ	450	500	450
$P_{t_\sigma}(\text{Cl})^\ddagger$	85	129	102
$F_{t_\sigma}(\text{Cl})$	22	9	0
$P_{t_\pi}(\text{Cl})$	78	82	86
$F_{t_\pi}(\text{Cl})$	9	12	18
$P_{t_\sigma}(\text{N})$	100	100	100
$F_{t_\sigma}(\text{N})$	38	35	33
$P_{t_{\pi//}}(\text{N})$	57	74	64
$F_{t_{\pi//}}(\text{N})$	18	19	19
$P_{t_{\pi\perp}}(\text{N})$	58	83	52
$F_{t_{\pi\perp}}(\text{N})$	3	12	17
$k\text{\S}$	0.82	0.85	0.85

† Energies (cm^{-1}).

‡ Dipole moments (10^{-2} debye).

\S No units.

Turning now to the propylenediamine chromophore, the same kinds of bond displacement are suggested by the schemes in figure 24. Once more, one factor due to chelation is proposed because of the small $\angle \text{N-Co-N}$ angle (88°) and another arises from the twisting of the donor nitrogen orbitals caused by the chelate conformation. Again, quantitative reproduction of the CD and other properties is achieved, though not uniquely, with parameter values that are similar to those in the sparteine chromophores. Representative details are given in table 11 and figure 21.

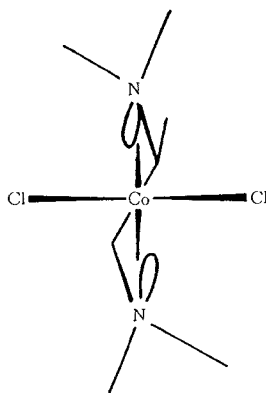


Figure 24. Origin of the optical chirality from bent bonding between metal and propylenediamine.

Finally consider the *S*-tan complexes of figure 20. Good reproduction of transition energies and absorbances were achieved with 'basic' parameter sets; but not of the circular dichroism. Each arm of the tripod ligand is much like the chelating amines in the preceding tetrahedral chromophores and, as mentioned above, they are arranged in a $\delta\delta\delta$ conformation. Once more, therefore, one can contemplate contributions to equatorial metal-amine bent bonding from both chelation strain and conformational twisting. As before, this would properly require augmentation of the parameter set with $e_{\pi//}$, $e_{\pi\perp}$, $e_{\pi\sigma//}$, $e_{\pi\sigma\perp}$, ${}^L t_{\pi//}$, ${}^L t_{\pi\perp}$ for the equatorial ligations. That degree of parameterization was too great in the tetrahedral species and we had to be content with semiquantitative values. The situation is much worse for the trigonal bipyramids which provide a much less rich data base. Instead, a number of trial calculations were made in which only one of these extra parameters was included: $e_{\pi\sigma//}$ or ${}^L t_{\pi//}$, where // means in the plane of each local M-N-C(H₂) moiety. It was found that a value for $e_{\pi\sigma//}$ of 50 cm⁻¹ for the cobalt species or of 80 cm⁻¹ for the nickel ones, together with very minor changes in the 'basic' parameter values provided an excellent account of the CD as well as intensities and transition energies. Typical parameter values are listed in tables 12 and 13. Equally good fits to experiment can be obtained instead with ${}^L t_{\pi//}$ values of about 1 to 2, for the cobalt system, or 2 to 3, for the nickel ones, on the scale of table 13.

While it is unfortunate that precise parameter values could not be established in these systems, some firm conclusions can be reached. First is that the CD experiment can only be reproduced with a recognition of some degree of misdirected valency. Parameterization by $e_{\pi\sigma//}$ does actually monitor contributions from both ring strain and conformational twisting as shown in figure 25. Bent bonding due to ring strain is illustrated in figure 25(a) and from twisting in figure 25(b). As $e_{\pi\sigma//}$ is defined with respect to the plane M-N-C(H₂), both effects contribute to this parameter. In short, parameterizations of the misdirected valency by $e_{\pi\sigma//}$ only is not wholly artificial. Secondly, the small magnitude required for $e_{\pi\sigma//}$ compared with that in the tetrahedral chromophores is consistent with our proposed view of the bent bonding in these two series. Thus, the preferred interbond angle at the metal in the tetrahedral species is close to 109° but in the trigonal bipyramidal ones it is 90°. So the contribution from ring strain in the latter system should be much less than in the former. We would argue that

Table 12. Ligand-field energy parameters (cm⁻¹) for the series, MLX; M = Co(II), Ni(II); L = *S*-tan; X = NCS, Cl, Br, I.

	CoLNCS	CoLCl	CoLBr	CoLI
$e_{\sigma}(\text{eq})$	3700	3800	3900	4100
$\bar{e}_{\pi}(\text{ax})\dagger$	4650	4300	4100	3800
$e_{\pi}(\text{X})$	1000	1200	1250	1250
$e_{\pi\sigma//}(\text{eq})$	50	50	50	50
	NiLNCS	NiLCl	NiLBr	NiLI
$e_{\sigma}(\text{eq})$	3500	3500	3600	3700
$\bar{e}_{\pi}(\text{ax})\dagger$	5300	5050	4900	4700
$e_{\pi}(\text{X})$	700	900	900	950
$e_{\pi\sigma//}(\text{eq})$	80	80	80	80

† Mean of $e_{\sigma}(\text{amine})$ and $e_{\sigma}(\text{X})$.

Table 13. Intensity parameters† for the series M(S-tan)X.

M	Co				Ni			
	X	NCS	Cl	Br	I	NCS	Cl	Br
$P_{t_\sigma}(\text{ax})\ddagger$	0	-92	-70	-83	34	-26	-36	-37
$F_{t_\sigma}(\text{ax})\ddagger$	43	-92	-70	-83	86	-26	-36	-37
$P_{t_\pi}(\text{X})$	16	0	7	0	17	0	7	0
$F_{t_\pi}(\text{X})$	8	12	7	16	17	0	0	0
$P_{t_\sigma}(\text{eq})$	0	0	0	0	5	0	0	0
$F_{t_\sigma}(\text{eq})$	11	12	14	16	34	34	36	37

† $L_{t_\lambda}(10^{-2}$ debye).

‡ $L_{t_\sigma}(\text{ax}) = L_{t_\sigma}(\text{X}) - L_{t_\sigma}(\text{N ax})$.

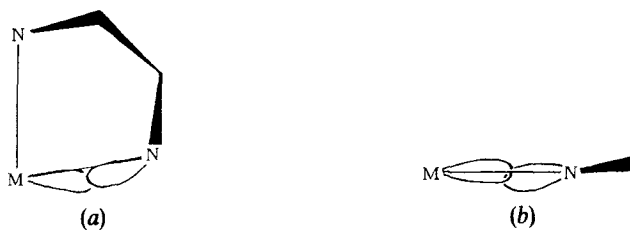


Figure 25. 'Side' and 'top' views of the bent bonding in the metal-propylenediamine interaction: (a) ring strain, (b) twisting.

it is just this sort of detailed consistency that encourages confidence in the whole ligand-field approach we have reviewed. In passing, we observe how these studies identify the sources of ligand-field perturbation as *bonds* rather than donor *atoms*.

In summary, then, structural chirality beyond the first coordination shells in these complexes communicates itself to the ligand-field d electron probe through bent bonding in the first coordination shell. Semiquantitatively, the details of this bent bonding are probed *consistently* by ligand-field analysis, making use of the same sort of ideas and trends that have served so well in our previous examples. While it is entirely possible to model optical activity within the so-called 'independent systems' framework and talk of 'coupling' between the d shell and ligand group functions, the present studies show that a simple and direct approach, once set up, can provide quantitative accounts of experiment using the language of everyday mainstream chemistry. The level of detail provided by the analyses of optical activity in the present systems not only illuminates our views of bent bonding but also suggests that the circumstances responsible for it may be widespread. Intimations of the contribution from ring strain were there in the early examples described in section 3: here it is demonstrated much more clearly. In the same way, in the early ligand-field analyses of a nominally tetrahedral Schiff base complex, a non-zero value for $e_{\pi//}(\text{O})$ presaged the idea of the ligand-field probe of non-bonding lone pairs. The indications were always there: with contemporary theoretical and computational power (and not a little patience) the detail is now exposed for all to see.

7. Concluding remarks

This has been an account of the evidence for bent bonding provided by modern ligand-field analyses. It has necessarily been a long account, for the power of the ligand-field method is often either unknown or doubted. It is sometimes suggested that their parametric nature confers upon ligand-field models a second-class status with respect to molecular-orbital schemes of various kinds. One must recognize, however, that no such computational approaches are presently able to account for the wide range of properties that characterize the 'ligand-field regime' with anything like the accuracy of the parametric ligand-field system. To justify this claim, however, it has been necessary, at the very least, to illustrate the detailed and repeated success of the ligand-field model when applied with the rigour and care that characterize modern studies. It is also important to state that many more analyses have been completed, with the same level of detail and success, on systems which would not be expected to, and did not, involve misdirected valency. In most of the studies described in this article, modelling without reference to misdirected valency was first shown to fail: subsequent success with its recognition is then even more persuasive. By extending the reach of ligand-field studies to electric-dipole intensities, to circular dichroism and, latterly, to magnetic circular dichroism, we have built a second level of parameterization, namely the t variables, with which one may confirm and augment the insight into chemical bonding provided by the more traditional means. The self-consistency of bonding views in transition-metal complexes gleaned from the e and t parameterizations in so wide a range of systems is one of the most encouraging aspects of these contemporary studies.

Acknowledgment

NDF thanks the U.K. SERC for a Research Studentship.

References

- BALLHAUSEN, C. J., and LIEHR, A. D., 1958, *J. molec. Spectrosc.*, **2**, 342.
BENCINI, A., BENELLI, C., GATTESCHI, D., and ZANCHINI, C., 1979, *Inorg. Chem.*, **18**, 2526.
BERTINI, I., GATTESCHI, D., and SCOZZOFAVA, A., 1976, *Inorg. Chem.*, **15**, 203.
BRINK, D. M., and SATCHLER, G. R., 1968, *Angular Momentum* (Oxford: Clarendon).
BROWN, C. A., GERLOCH, M., and McMEEKING, R. F., 1988a, *Molec. Phys.*, **64**, 771.
BROWN, C. A., DUER, M. J., GERLOCH, M., and McMEEKING, R. F., 1988b, *Molec. Phys.*, **64**, 793; 1988c, *Ibid.*, **64**, 825.
CHANDLER, G. S., FIGGIS, B. N., PHILLIPS, R. A., REYNOLDS, P. A., and WILLIAMS, G. A., 1982, *Proc. R. Soc.*, **A384**, 31.
CRUSE, D. A., and GERLOCH, M., 1977, *J. chem. Soc., Dalton Trans.*, 152.
DALE, A. R., DUER, M. J., FENTON, N. D., GERLOCH, M., and McMEEKING, R. F., 1989, *CAMMAG3*, A FORTRAN programme suite.
DAUL, C., SCHLÄPFER, C. W., and VON ZELEWSKY, A., 1979, *Struct. Bonding, Berlin*, **36**, 129.
DEETH, R. J., and GERLOCH, M., 1984, *Inorg. Chem.*, **23**, 3846; 1987, *Ibid.*, **26**, 2582.
DEETH, R. J., DUER, M. J., and GERLOCH, M., 1987a, *Inorg. Chem.*, **26**, 2573; 1987b, *Ibid.*, **26**, 2578.
DEVLIN, M. T., STEPHENS, E. M., RICHARDSON, F. S., VAN COTT, T. C., and DAVIS, S. A., 1987a, *Inorg. Chem.*, **26**, 1204.
DEVLIN, M. T., STEPHENS, E. M., REID, M. F., and RICHARDSON, F. S., 1987b, *Inorg. Chem.*, **26**, 1208.
DUER, M. J., and GERLOCH, M., 1989a, *Inorg. Chem.*, **28**, 4260; 1989b, *J. chem. Soc., Dalton Trans.*, 2109; 1990, *Molec. Phys.* (submitted).
FALVELLO, L. R., and GERLOCH, M., 1981, *Inorg. Chem.*, **19**, 472.
FALVELLO, L. R., GERLOCH, M., and RAITHY, P. R., 1987, *Acta. crystallogr.*, **C**, **43**, 2029.
FENTON, N. D., and GERLOCH, M., 1987, *Inorg. Chem.*, **26**, 3273; 1989a, *Ibid.*, **28**, 2767; 1989b, *Ibid.*, **28**, 2975; 1990a, *Inorg. Chem.* (submitted); 1990b, *Inorg. Chem.* (submitted).
GERLOCH, M., 1983, *Magnetism and Ligand-Field Analysis* (Cambridge University Press).

- GERLOCH, M., 1987, *Understanding Molecular Properties*, Vol. 111, edited by J. S. Avery, J. P. Dahl and A. Hansen (Dordrecht: Reidel); 1990, *Coord. Chem. Rev.* (to be published).
- GERLOCH, M., HARDING, J. H., and WOOLEY, R. G., 1981, *Struct. Bonding*, **46**, 1.
- GERLOCH, M., and WOOLLEY, R. G., 1984, *Prog. Inorg. Chem.*, **31**, 371.
- GILLESPIE, R. J., and NYHOLM, R. S., 1957, *Quart. Rev. Chem. Soc.*, **11**, 339.
- HITCHMAN, M. A., 1974, *Inorg. Chem.*, **13**, 2218.
- JUDD, B. R., 1962, *Phys. Rev.*, **127**, 750; 1979, *J. chem. Phys.*, **70**, 4830.
- LEVER, A. B. P., WALKER, I. M., MCCARTHY, P. J., MERTES, K. B., JIRCITANO, A., and SHELDON, R., 1983, *Inorg. Chem.*, **22**, 2252.
- MASON, S. F., PEACOCK, R. D., and STEWART, B., 1975, *Molec. Phys.*, **30**, 1829.
- OFELT, G. S., 1962, *J. chem. Phys.*, **37**, 511.
- PAULING, P., ROBERTSON, G. B., and RODLEY, G. A., 1965, *Nature*, **207**, 73.
- RICHARDSON, F. S., 1979, *Chem. Rev.*, **79**, 17.
- STEPHENS, E. M., DAVIS, S., REID, M. F., and RICHARDSON, F. S., 1984a, *Inorg. Chem.*, **23**, 4607.
- STEPHENS, E. M., REID, M. F., and RICHARDSON, F. S., 1984b, *Inorg. Chem.*, **23**, 4611.
- VARGHESE, J. N., and MASLEN, E. N., 1985, *Acta crystallogr. B*, **41**, 184.
- WOOLLEY, R. G., 1981, *Molec. Phys.*, **42**, 703; 1985, *Chem. Phys. Lett.*, **118**, 207; 1987, *Int. Rev. phys. Chem.*, **6**, 93.